NUCLEAR STRUCTURE -- EXPERIMENTAL

SINGLE-NUCLEON TRANSFER AND INELASTIC SCATTERING REACTIONS WITH RADIOACTIVE BEAMS

R. A. Kryger, A. Azhari, M. Hellström, J.H. Kelley, T. Kubo, R. Pfaff, E. Ramakrishnan, B.M. Sherrill, M. Thoennessen, S. Yokoyama, R.J. Charity[a], J. Dempsey[a], A. Kirov[a], N. Robertson[a], D.G. Sarantites[a], L.G. Sobotka[a], and J.A. Winger[b]

Production and identification of nuclei away from the line of stability is difficult due to small cross sections and large backgrounds associated with competing reactions. Consequently, complex fragment separators such as the A1200 have been constructed which can select out weakly populated fragments. However, the large background of reaction products can significantly complicate the detection of decay products of weakly populated fragments if the fragment lifetimes are short compared to the transit time through a fragment separator. With an interest in the investigation of nuclei beyond the proton dripline, as well as particle-unbound states of proton-rich nuclei, we have studied the use of single-nucleon transfer reactions and inelastic scattering using a radioactive beam as a means to populate states of interest. This method offers the advantage of well-understood kinematics in a reaction environment with a limited number of strong background reactions. Unfortunately, cross section measurements of transfer reactions with radioactive projectiles are rare, but estimates can be made based upon systematics for light nuclei.

Our first test was to study the $^{13}O + ^{9}Be$ reaction. The primary motivation for this reaction choice was to investigate the ground state two proton decay of ^{12}O populated via neutron stripping. Ground state two-proton emission occurs in particle-unbound proton-rich nuclei when the two-proton decay channel is energetically allowed but one proton emission is forbidden or strongly suppressed. Of particular interest is the investigation of whether the decay takes place through a direct 3-body mechanism, ^{2}He emission, or sequential one proton emission when possible. In addition to ^{12}O formed via neutron stripping, we also expect neutron pickup and proton stripping reactions leading to states in ^{14}O and ^{12}N, as well as inelastic scattering to states in ^{13}O itself.

The ^{13}O beam was produced in the fragmentation of 80 MeV/A ^{16}O from the K1200 cyclotron on a 1000 mg/cm^2 Be primary target. The intensity of the primary beam varied between 150 and 200 pnA. The secondary beam was separated using the A1200 fragment separator and further purified within the Reaction Product Mass Separator (RPMS). A thin plastic scintillator behind the RPMS was used to measure the secondary beam time-of-flight (TOF) relative to the cyclotron RF signal. In conjunction with a silicon detector ΔE signal, the purity of the ^{13}O beam was determined to be $> 95\%$ with a small contamination of ^{12}N. During the coincidence runs, the silicon detector was removed and the beam identification was monitored particle-by-particle using the TOF signal. Two position sensitive parallel plate avalanche counters (PPAC) separated by 1 m were placed in the beam path just before the secondary target in order to track the ^{13}O particles incident on the 47 mg/cm^2 secondary ^{9}Be target. This thickness was limited by the effect of the target energy loss on the $2p + ^{10}C$ relative energy resolution. The final ^{13}O beam intensity varied between 2000 and 5000 cps, depending on the beam transmission efficiency and the primary beam intensity. The energy of the secondary ^{13}O beam was 33.4 MeV/A incident on the secondary target, and the beam spot size was approximately 1 cm (FWHM).

Heavy reaction products and the energy-degraded secondary beam were detected in a ΔE-E silicon telescope placed 84 cm downstream of the target, directly at 0°. The ΔE detector consisted of a 5 cm by 5 cm square MICRON double-sided strip detector with 16 vertical strips on the front and 16 horizontal

strips on the back. The detector thickness was 304 μm and the strips yielded x-y position information in addition to energy-loss. The E detector consisted of a 6.5 cm diameter 3 mm thick Si(Li) detector with four pie-shaped segments. Isotope identification was achieved using the ΔE-E information and the total fragment energy was determined from the sum of the two detector energies. The fragment telescope was calibrated using ^{10}C beams produced at several energies using the A1200 fragment separator. A final energy resolution of 1% was obtained for ^{10}C fragments. Coincident protons were detected in the Washington University MINIWALL detector array positioned approximately 60 cm downstream of the target. This detector array consisted of 112 CsI detectors arranged in 5 rings around the beam axis covering laboratory angles between 3° and 12°. Each ring contained between 16 and 24 detectors so that proton position was determined in addition to energy. Proton signals were distinguished from other light particles using pulse shape techniques. The detectors were energy calibrated using proton beams produced at 35 MeV and 70 MeV in combination with several energy-degrading foils.

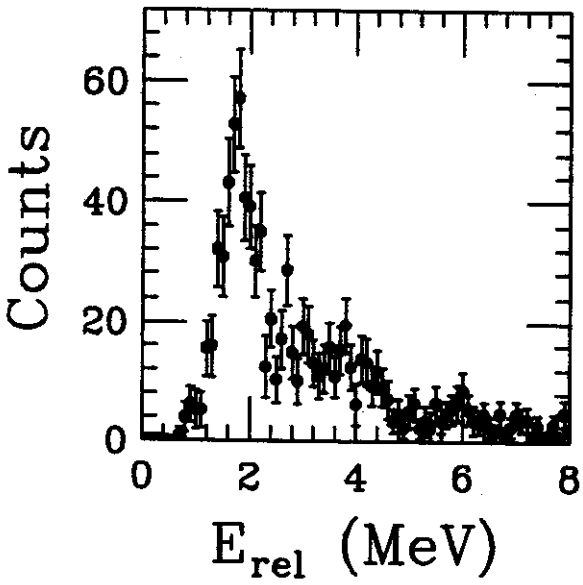

Figure 1: A plot of the relative energy in the three-particle center-of-mass for the 2p + ^{10}C coincidence events.

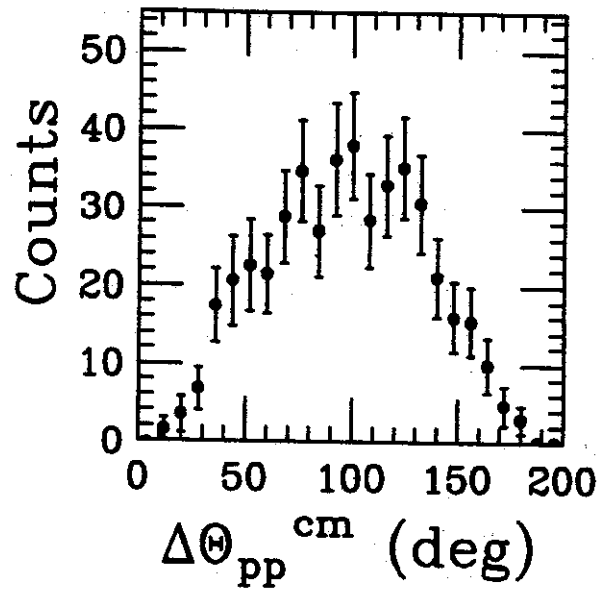

Figure 2: The opening angle distribution between the two protons evaluated in the three-particle center of mass for the 2p + ^{10}C events.

Figure 1 shows the relative energy spectrum obtained for the 2p + ^{10}C coincidence events. A sharp peak is seen centered at energy 1.80 MeV with a FWHM of 750 keV. After subtraction of the experimental resolution ($\sim$ 600 keV), these values are consistent with the previously measured ^{12}O energy 1.78(40) MeV and width 450(250) keV[1]. Some evidence is also seen for higher-lying states in ^{12}O, although the resolution worsens with increasing relative energy. The opening angle distribution for protons evaluated in the three-particle center-of-mass is shown in Figure 2. These data are gated on the ground state ^{12}O peak in Figure 1. The data show no evidence for a small-angle enhancement as might be expected from the ^{2}He decay mode of ^{12}O. Rather, the data seem to indicate an isotropic emission of the two protons suggesting that either direct three-body decay or sequential one-proton emission through ^{11}N appears to

dominate. A more quantitative analysis of these data are in progress.

In addition to the ^{12}O decay products, we also analyzed events with one proton in coincidence with ^{12,13}N and ^{11}C. Figure 3 shows the relative energy for the 1p + ^{11}C data which was the strongest reaction channel we observed. The solid line in Figure 3 is the result of a Monte Carlo simulation modeling the decay of the first three (proton-unbound) excited states of the proton-stripping reaction product ^{12}N. The simulation used the known energies and widths of these states and incorporated the geometrical acceptance and the detector resolutions. The dotted lines in the Figure show the individual contributions due to the three states. The relative strength of the three contributions as well as the absolute normalization was obtained by χ^2 minimization. This procedure gives a good fit to the data and allows us to extract population cross sections for the ^{12}N states. The observation of proton-unbound ^{13}O states (see below) indicates that not all of the ^{12}N population is directly due to proton-stripping reactions from the ^{13}O.

Figure 4 shows the relative energy spectrum for the 1p + ^{13}N events. Here again, the solid line shows a model simulation of the neutron-pickup nucleus ^{14}O which includes the first five well known excited states. The individual contributions are shown as dotted curves. The fit is quite good except for the enhanced counts in the data near 2.8 MeV. This probably corresponds to one or more excited states in ^{14}O which have not been reported before.

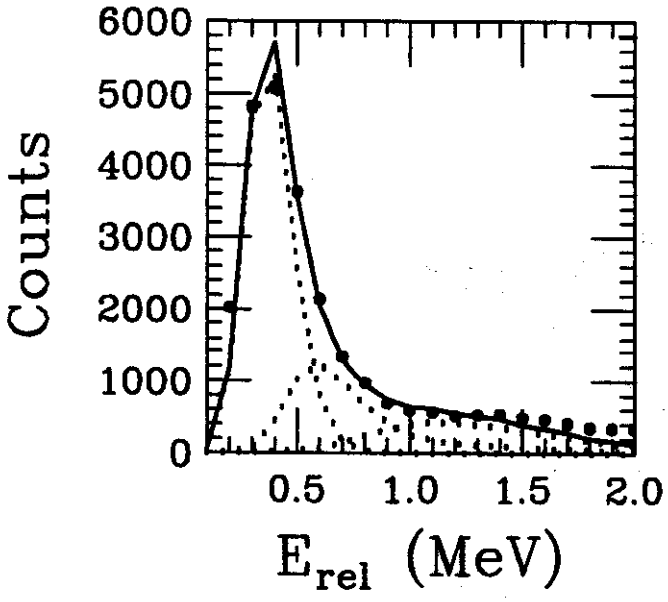

Figure 3: The relative energy spectrum for the ^{11}C + 1p data. The solid and dotted lines are the result of a Monte Carlo simulation discussed in the text.

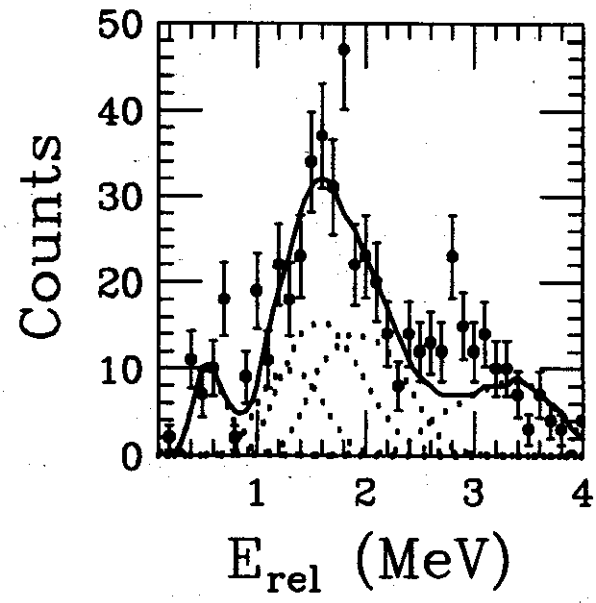

Figure 4: The relative energy spectrum for the ^{13}N + 1p data.

Figure 5 shows the relative energy spectrum for the 1p + ^{12}N coincident events. We used model simulations of the decay of the first two excited states of ^{13}O to compare with the data, but in this case no width information had been reported for these states. By optimizing our Monte Carlo simulations to fit the data, we remeasured the excitation energies and were also able to obtain the widths of these two

states. The solid and dashed lines show the results of our best fit which yielded an ^{13}O excitation energy of 2.66(15) MeV and width 690(450) keV for the first state and an excitation energy and width of ~4 MeV and ~1 MeV, respectively, for the second state. These latter values are best fit values and the uncertainties are relatively large.

In conclusion, we have reported the results of our study of several proton-unbound nuclear states in $^{12,13,14}O$ and ^{12}N formed via neutron stripping and pickup, proton pickup, and inelastic scattering using a ^{13}O projectile. Measured relative energy spectra from proton-fragment coincidences have been analyzed by comparison with Monte Carlo simulations of the decaying states and properties of states such as energies and widths can be determined in addition to relative populations of states in these single-particle transfer reactions. In addition, a decay study of the ground state two proton emitter ^{12}O was completed by observation of the 2p + ^{10}C decay products and the proton angular correlations suggest isotropic proton emission in the three-particle center-of-mass.

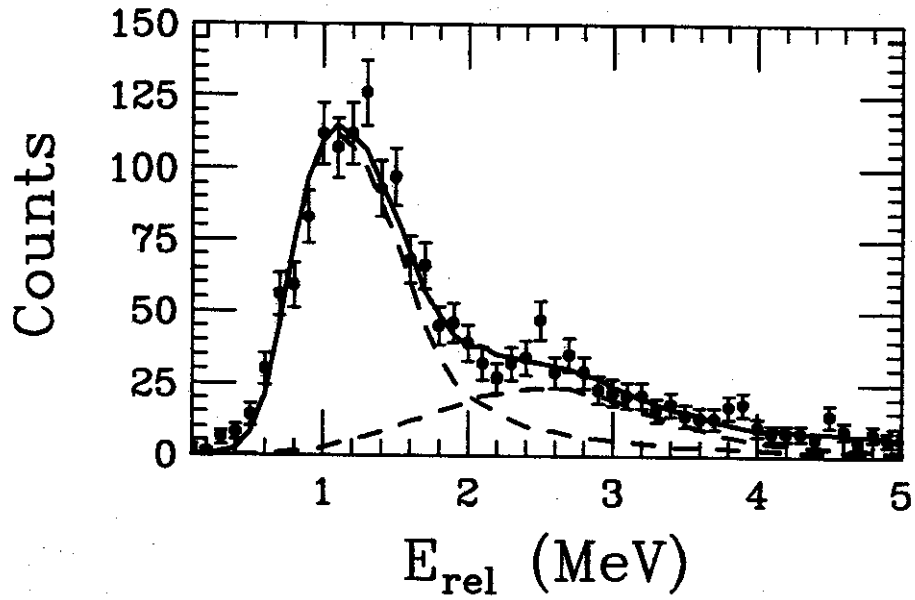

Figure 5: The relative energy spectrum for the ^{12}N + 1p data.

a. Department of Chemistry, Washington University, St. Louis, MO 63130.
b. Cyclotron Institute, Texas A & M University, College Station, TX 77843.

References

1. F. Ajzenberg-Selove, Nucl. Phys. A523, 1 (1991).

SEQUENTIAL NEUTRON DECAY SPECTROSCOPY OF ^{10}Li

S. Yokoyama, A. Azhari, W. Benenson, A. Galonsky, J. H. Kelley, R. A. Kryger, T. Kubo[a], D. J. Morrissey, R. Pfaff, E. Ramakrishnan, B. M. Sherrill, and M. Thoennessen

In the last few years major experimental efforts have been devoted to the study of ^{10}Li. Especially the energy of the ground state or the mass of ^{10}Li is of high current interest because it is an essential ingredient for the understanding of the halo nucleus ^{11}Li. The three-body interaction in ^{11}Li, i.e. ^{9}Li-n-n is based on the underlying two-body interactions n-n, and n-^{9}Li which is ^{10}Li. Several different experimental approaches, for example multi-nucleon transfer reactions [1-3] and pion absorption measurements [4] yielded conflicting values for the mass of ^{10}Li. The decay energy of the ground state varied from 150 to 800 keV.

We used the technique of Sequential Neutron Decay Spectroscopy [5] applied for the first time at zero degrees in order to extract the decay energy of ^{10}Li [6]. In this method, ^{10}Li nuclei are produced with a fragmentation reaction, and the decay energy is derived from the relative velocity of the decay product (^{9}Li) and the coincident neutron. We observed a small decay energy of <300 keV which was recently confirmed by an independent measurement which used essentially the same method [7].

Our first experiment had only limited energy and time resolution, and thus we repeated our measurement with improved resolution. A 94 mg/cm^2 ^{9}Be target was bombarded with an 80 MeV/nucleon ^{18}O beam, and the fragmentation product and the scattered beam were separated with a quadrupole/dipole combination. The ^{9}Li fragments from the decay of ^{10}Li were detected in a detector telescope consisting of a thin plastic timing scintillator, a 16x16 silicon strip ΔE detector, and a thick plastic scintillator for the total energy measurement. The dipole magnet was optimized to focus fragments with a mass-to-charge ratio of three (^{9}Li). Thus we were able to collect simultaneously calibration data from the decay of ^{7}He to ^{6}He and a neutron. Neutrons were detected in coincidence at zero degrees with an array of fourteen BaF_2 scintillators and one NE213 liquid scintillator.

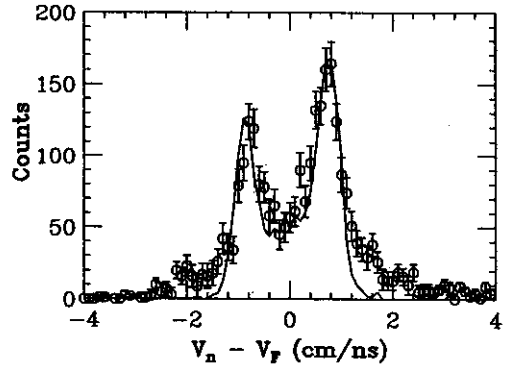

Figure 1: Relative velocity spectrum of ^{6}He fragments and neutrons from the decay of ^{7}He. The solid line shows a Monte Carlo simulation.

The overall energy resolution of the fragment detector was ~4.5%. However a position dependent calibration, with help of the strip detector, improved the resolution to ~2.4%. The neutron

velocity was derived from time-of-flight information measured with respect to the fragment detector. Thus the time measurement was independent of the rf timing of the cyclotron.

Figure 1 shows the relative velocity spectrum of the ^{7}He decay. The solid line is the result of a Monte Carlo simulation which included the known decay properties of ^{7}He, the experimental geometry and detector efficiencies, as well as the timing and energy resolutions. The good fit to the data was achieved with an overall energy resolution of the decay energy of 167 keV compared to 287 keV in the previous experiment.

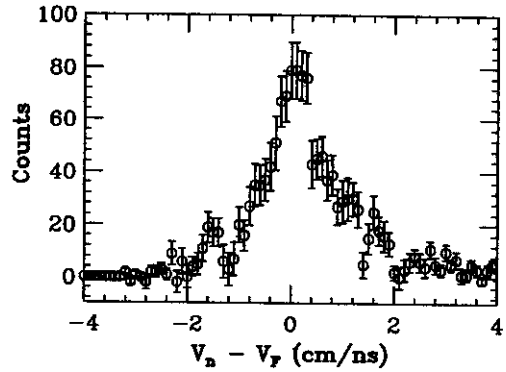

Figure 2: Relative velocity spectrum of the ^{10}Li decay.

The relative velocity spectrum of the ^{10}Li decay is shown in Figure 2. The single central peak indicates the presence of a rather small decay energy and confirms our previous measurements. Detailed Monte Carlo simulations are currently under way. However, the width of this peak is essentially identically to the width observed in the first experiment and thus indicates that it is not dominated by the experimental resolution but by the width of the state.

a. RIKEN, Wako, Saitama, Japan

References

1. K. H. Wilcox *et al.*, Phys. lett. **59B** 142 (1975)
2. H. G. Bohlen *et al.*, Z. Phys. **A344** 381 (1993)
3. B. M. Young *et al.*, Phys. Rev. C **49** 279 (1994)
4. A. I. Amelin *et al.*, Sov. J. Nucl. Phys. **53** 782 (1990)
5. F. Deák *et al.*, Nucl. Instrum. Methods **A258** 67 (1987)
6. R. A. Kryger *et al.*, Phys. Rev. C **47** R2439 (1993)
7. T. Kobayashi *et al.*, Proc. of the 3rd Int. Conf. on Radioactive Nuclear Beams (East Lansing, USA, May 1993), D. J. Morrissey, Ed., Edition Frontières (Gif-sur-Yvette, France, 1993) 169

THE LORENTZIAN DISTRIBUTION AND THE EFFECT OF A LIMITED ACCEPTANCE WHEN MEASURING FRAGMENT MOMENTUM DISTRIBUTIONS FROM HALO NUCLEI

J.H. Kelley, Sam M. Austin, T. Kubo[a], N.A. Orr[b], and B.M. Sherrill

The surprisingly large matter radii derived from the interaction cross sections of light neutron rich nuclei [1] have recently inspired interest in the structure of these weakly bound particles. The enhanced cross sections are explained by assuming the weakly bound valence neutron(s) form a diffuse layer around a more tightly bound core. For example, in the case of ^{11}Li the two valence neutrons have a *rms* radius of 5.8 fm while the *rms* radius of the ^{9}Li core is 2.32 fm. The halo effect is understood by considering the wave function of the neutron outside the potential well of the core. Hansen and Jonson [2] explain that in this region the wave function decays exponentially with a decay length ρ, where $\rho = \hbar/\sqrt{2\mu S_n}$ =8.2 fm for ^{11}Li. Here the wave function can be approximated with a Yukawa wave function,

$$\Psi(\vec{r}) = \sqrt{2\pi\rho}\,\frac{\exp(-r/\rho)}{r}.$$

The narrow momentum distribution of ^{9}Li fragments (FWHM≈45 MeV/c) from the break up of ^{11}Li [3] is different from fragmentation of normal nuclei. It is not described by the standard Goldhaber model, which relates the Gaussian width of the fragment momentum distribution (FWHM=2.355σ) to the Fermi momentum ($P_{Fermi}=\hbar/(1.2A^{1/3})$) of the incoming projectile,

$$\sigma = \frac{P_{Fermi}}{\sqrt{5}}\sqrt{\frac{A_{fragment}(A_{projectile}-A_{fragment})}{A_{projectile}-1}}.$$

It is believed that the ^{9}Li fragment momentum distribution reflects, via the quantum mechanical relation between position and momentum, the spatial distribution of the halo neutrons. Since the Fourier transform of the Yukawa radial wave function leads to a Lorentzian momentum wave function,

$$\Psi(\vec{p}) = \sqrt{\frac{\hbar}{\rho\pi^2}}\,\frac{1}{\vec{p}^2+(\hbar/\rho)^2} = \sqrt{\frac{\Gamma}{2\pi^2}}\,\frac{1}{\vec{p}^2+(\Gamma/2)^2},$$

a Lorentzian approach to evaluating the ^{9}Li fragment momentum distribution is a reasonable first approximation. With this assumption the experimental results of Orr *et al.* [3] suggest a *rms* radius of 6.2 fm in agreement with the value of 5.8 fm [4].

Measurements of the fragment momentum distributions from ^{12}C, ^{14}N and ^{16}O, *i.e.* [5], show that Gaussian distributions best represent the shape of the fragment momentum distributions in normal matter. However if the momentum distribution is non-Gaussian (e.g. Lorentzian) there can be subtle changes in the observed momentum distribution caused by the finite acceptance for fragments. The effect is rooted in a dependence between the Cartesian components of the Lorentzian momentum density distribution. In principle this is most important when a limited acceptance prevents a complete collection of the break up fragments. For a simple form like the Lorentzian distribution the dependence is well understood and analytical solutions for the momentum distribution following a limited acceptance can be obtained. Henceforth we will focus on two points relevant to measuring momentum distributions when a Lorentzian density distribution is involved. The first is a complete analytical solution giving the predicted line shape of a Lorentzian distribution after passing through a limited acceptance. The second relates to features of a Lorentzian distribution that can be observed using very simple techniques.

After passing through the angular and momentum acceptance of a device the resulting parallel momentum distribution can be obtained by integration of the momentum density distribution of the break up fragments over the range of momenta falling inside the acceptance. We make some approximations to simplify the mathematics. Since the width of the fragment momentum distribution is small for a halo nucleus, the total momentum of the fragment is approximately equal to its parallel momentum ($p \approx p_z$). Hence we assume the transverse momentum cut-offs are given by $Px_{\lim} = P_z^{ave} \sin(\Delta\theta/2)$ and $Py_{\lim} = P_z^{ave} \sin(\Delta\phi/2)$ for a square acceptance that is symmetric with respect to 0°. Then the fragment parallel momentum distribution in the lab frame is,

$$\int_{-px_{\lim}}^{px_{\lim}} \int_{-py_{\lim}}^{py_{\lim}} \rho(\vec{p})\mathrm{d}px\mathrm{d}py = \int_{-px_{\lim}}^{px_{\lim}} \int_{-py_{\lim}}^{py_{\lim}} |\Psi(\vec{p})|^2 \mathrm{d}px\mathrm{d}py$$

$$\propto \int_{-py_{\lim}}^{py_{\lim}} \int_{-px_{\lim}}^{px_{\lim}} \frac{\mathrm{d}px\mathrm{d}py}{\left[p_x^2 + p_y^2 + \left(p_z - p_z^{ave}\right)^2 + (\Gamma/2)^2\right]^2}$$

$$\propto \int_{-py_{\lim}}^{py_{\lim}} \left\{ \frac{px_{\lim}}{\left[py^2 + \left(p_z - p_z^{ave}\right)^2 + (\Gamma/2)^2\right]\left[px_{\lim}^2 + py^2 + \left(p_z - p_z^{ave}\right)^2 + (\Gamma/2)^2\right]} + \frac{\mathrm{Arctan}\left(\dfrac{px_{\lim}}{\sqrt{py^2 + \left(p_z - p_z^{ave}\right)^2 + (\Gamma/2)^2}}\right)}{\left[py^2 + \left(p_z - p_z^{ave}\right)^2 + (\Gamma/2)^2\right]^{3/2}} \right\} \mathrm{d}py$$

$$\propto \left\{ \frac{py_{\lim}\, A\mathrm{rctan}\left(\dfrac{px_{\lim}}{\sqrt{py^2 + \left(p_z - p_z^{ave}\right)^2 + (\Gamma/2)^2}}\right)}{\left(\left(p_z - p_z^{ave}\right)^2 + (\Gamma/2)^2\right)\sqrt{py_{\lim}^2 + \left(p_z - p_z^{ave}\right)^2 + (\Gamma/2)^2}} - \frac{2\,\mathrm{Arctan}\left(\dfrac{py_{\lim}}{\sqrt{\left(p_z - p_z^{ave}\right)^2 + (\Gamma/2)^2}}\right)}{px_{\lim}\sqrt{\left(p_z - p_z^{ave}\right)^2 + (\Gamma/2)^2}} + \frac{\sqrt{px_{\lim}^2 + \left(p_z - p_z^{ave}\right)^2 + (\Gamma/2)^2}\ \mathrm{Arctan}\left(\dfrac{py_{\lim}}{\sqrt{px_{\lim}^2 + \left(p_z - p_z^{ave}\right)^2 + (\Gamma/2)^2}}\right)}{px_{\lim}\sqrt{\left(p_z - p_z^{ave}\right)^2 + (\Gamma/2)^2}} \right\}$$

In the limit of an infinite acceptance the above does reduce to the expected Lorentzian shape,

$$\int_{-\infty}^{\infty} \int_{-\infty}^{\infty} \rho(\vec{p})\mathrm{d}px\mathrm{d}py = \frac{\Gamma}{2\pi} \frac{1}{\left(p_z - p_z^{ave}\right)^2 + (\Gamma/2)^2}.$$

We can also easily derive the formula used when measuring the transverse momentum distribution,

$$\int_{-\infty}^{\infty} \rho(\vec{p})\mathrm{d}p_{parallel} = \frac{\Gamma}{4\pi} \frac{1}{\left[p_{transverse}^2 + (\Gamma/2)^2\right]^{3/2}}.$$

Our interest lies in understanding what influence the limited acceptance of the A1200 may have on measurements of the fragment momentum distributions from halo nuclei. We show in

figure 1 the expected parallel momentum distribution of a 10 *amu* nucleus whose mean momentum is 3400 MeV/c and whose momentum distribution is Lorentzian with width parameter is $\Gamma = 50$ MeV/c. The solid line is expected with an infinite acceptance, the long dashed line takes into consideration the acceptance of the part of the A1200 following the breakup target at the Image 2 target box ($\Delta\theta = 40$ mrad and $\Delta\phi = 20$ mrad). To show the differences between the full acceptance and limited acceptance the short dashed line is the limited acceptance case scaled to match the height of the infinite acceptance case (*i.e.* 1.277 times the long dashed line). The full width at half maximum (FWHM) for an infinite acceptance is 50 MeV/c, however the influence of a limited acceptance causes the distribution width to narrow by 15% to 43.1 MeV/c while also decreasing the size of the tails. It remains unclear to what extent this result applies to the physical situation. It is a constructive exercise to consider a Lorentzian approximation for the wave function, though the wave function is more complex than a simple Lorentzian and we feel more sophisticated models should be used when making assumptions of how the data is influenced by the experimental conditions.

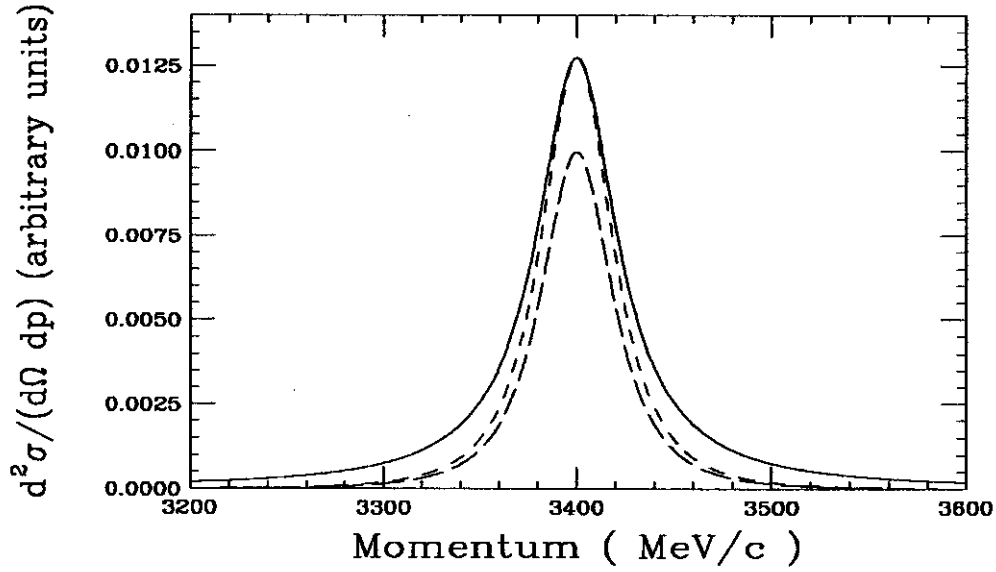

Figure 1: The parallel momentum distribution from a 10 *amu* fragment whose Lorentzian momentum distribution width parameter is Γ=50 MeV/c. The solid line is for an infinite acceptance, the long dashed line is expected when the Image 2 target pot determines the fragment acceptance. The short dashed line is the limited acceptance case (long dashed line) scaled to the full height if the infinite acceptance case to clarify the nature of the change in shape.

Next we consider the dependence that exists between the parallel and transverse components of a Lorentzian momentum distribution. If we assume the acceptance is a pin hole, the observed parallel momentum distribution, $P(p_{parallel})$, is given by,

$$P(p_{parallel}) = \iint_{\text{pin hole}} \rho(\vec{p})\,dp_x dp_y = \frac{\Gamma}{2\pi^2} \frac{1}{\left[\left(p_{parallel} - p^{ave}_{parallel}\right)^2 + p_\perp^2 + (\Gamma/2)^2\right]^2}.$$

Where $p_\perp$ is nearly a constant defined by $p_\perp = p^{ave}_{parallel} \sin(\theta_{acceptance})$ and $\theta_{acceptance}$ is the detector angle with respect to the beam. It is a simple algebraic step to show that the FWHM of the parallel momentum distribution, $P(p_{parallel})$, is,

$$\mathrm{FWHM} = 2\sqrt{\sqrt{2}-1}\sqrt{p_{\perp}^2 + (\Gamma/2)^2}\,.$$

In the limit that the pin hole is placed at zero degrees the FWHM is 0.64Γ, while for large angles the FWHM of the parallel momentum distribution has a linear dependence on the transverse momentum.

In figure 2 we show graphically the dependence of the width of the parallel momentum distribution on the transverse momentum expected from an aperture the size of the S320 acceptance for a Lorentzian momentum distribution (solid line) and for a Gaussian momentum distribution (dashed line, no acceptance dependence is expected).

The data shown are from a recent Kubo *et al.* [6] experiment studying the break up of 37A MeV ^{11}Li in Be and U targets with the S320. The Be target data closely follow the trend predicted for a Lorentzian momentum density distribution. Excitation and subsequent decay of a low lying state is inconsistent with the Be target data, supporting the notion that the measured ^{9}Li momentum distribution is the result of a direct breakup into the continuum, reflecting the initial state ^{9}Li momentum distribution. The data from the U target are in better agreement with a Gaussian momentum density distribution and require a more rigorous experimental setup for complete interpretation. Large Coulomb deflection and multiple scattering associated with the thick U target could possibly explain the result (soon to be answered via Monte Carlo simulation), though excitation of a low lying soft dipole state [7], representing the oscillation of the halo neutrons against the core, could also contribute to the deviation from the Lorentzian prediction.

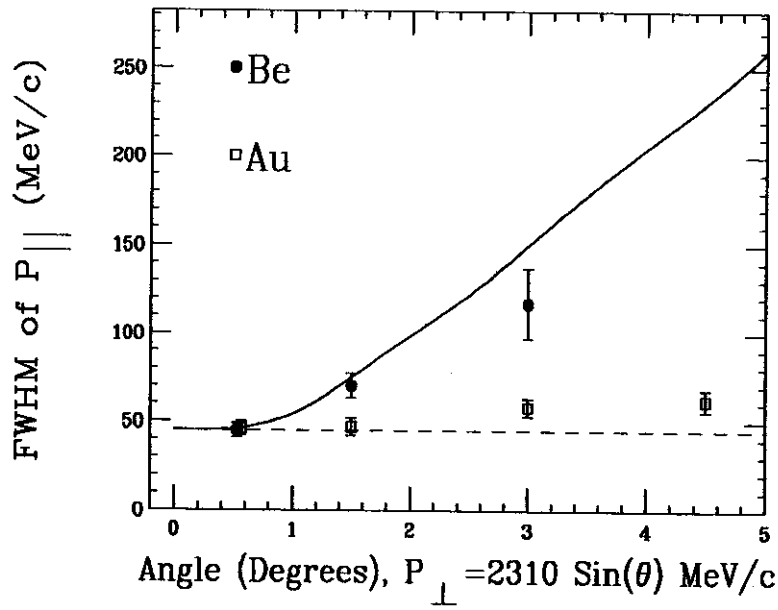

Figure 2: The expected parallel momentum distribution from a Lorentzian density distribution (solid), a Gaussian density distribution (dashed), compared with data from the breakup of ^{11}Li in the S320 from Kubo *et al.*

In summary, we have given the solution for the expected parallel momentum distribution resulting from the break up of a nucleus whose fragments are emitted with a Lorentzian distribution and detected with a device having a limited acceptance. Coupling between the Cartesian components of the Lorentzian distribution can cause the "post" acceptance distribution to deviate from the distribution for a device having an infinite acceptance. A comparison with data from the break up of ^{11}Li on a Be target shows only a slight deviation from the prediction assuming

a Lorentzian distribution. We expect that the deviation arises due to differences between the simple Yukawa model used and the actual wave function for the neutrons. The inspiration for this work is related to communications with Karsten Riisager and his work on this subject [8]

a. RIKEN(The Institute of Chemical and Physical Research), Wako, Saitama, 351-01, Japan
b. LPC, Boulevard du Marechal Juin, 14050 Caen Cedex, France

References

1. I. Tanihata *et al.*, Phys. Lett. B **206** (1988) 592.
2. P.G. Hansen and B. Jonson, Europhysics Letters **4** (1987) 409.
3. N.A. Orr *et al.*, Phys. Rev. Lett. **69** (1992) 2050.
4. H. Esbensen, Phys Rev. C **44** (1991) 440.
5. J.M. Kidd *et al.*, Phys. Rev. C **37** (1988) 2613.
6. T. Kubo *et al.*, Private comm.
7. D. Sackett, *et al.*, Phys. Rev. C **48** (1993) 118.
8. K. Riisager, Proceedings of the 3rd International Conference on Radioactive Nuclear Beams, East Lansing, Michigan, (1993), 281.

A METHOD FOR APPROXIMATING THE EFFECT OF A LIMITED ACCEPTANCE WHEN MEASURING FRAGMENT MOMENTUM DISTRIBUTIONS FROM HALO NUCLEI

J.H. Kelley and Sam M. Austin

Measurements of the parallel momentum ($p_{\parallel}$) distribution of fragments following direct breakup have been conducted as a probe of the wave function of valence nucleons in halo nuclei (for example see [1]). The shape of $p_{\parallel}$ distributions can be influenced by transverse acceptance limits if dependencies exist between the Cartesian components of the momentum density distribution [2]. It is often difficult to apply the corrections for a limited acceptance directly to the theory, for example because of nontrivial integrals of the momentum density distribution over the transverse limits. However, these integrals are possible for a Lorentzian distribution (the Fourier transform of a Yukawa wave function), and the analytical solution showing the effect of a limited acceptance on a Lorentzian momentum density distribution is shown in detail in Ref [3]. We develop here a technique based on the superposition of Gaussians, fit to a theoretical lineshape, to approximate the influence of a limited acceptance. We fit three Gaussian distributions to the predicted $p_{\parallel}$ distribution, find the transmission for each individual Gaussian, then construct the post acceptance distribution taking into account the incomplete transmission of larger width distributions.

If a linear combination of three-Gaussian distributions can duplicate a theoretically derived distribution by having closely the same probabilities for all important momenta in three dimensional space, $P(p_x,p_y,p_z)$, then the two distributions will give the same observations when studied, independent of what transformation, cut, or other operation is applied to the distribution.

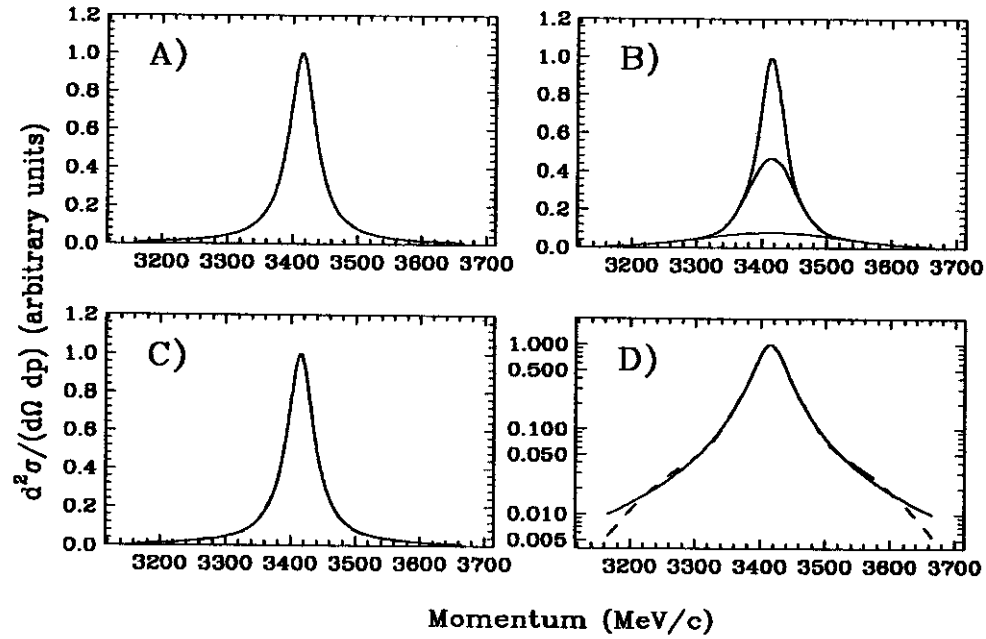

Figure 1. A comparison of a Lorentzian distribution (A), Γ=50, and a three Gaussian best fit to the Lorentzian (B). Figs 3C and 3D give a direct comparison of the Lorentzian (solid) and the fit (dashed).

Figure 1 compares a Lorentzian $p_{\parallel}$ distribution (Γ=50 MeV/c) with the three-Gaussian best fit. If the distribution is written in the form of,

$$3\text{-}G=A\exp(-p^2/(2\sigma_1^2)) + B\exp(-p^2/(2\sigma_2^2)) + C\exp(-p^2/(2\sigma_3^2)),$$

then A=0.5254, B=0.3886, and C=0.0789, and σ_1=14.63 MeV/c, σ_2=34.10 MeV/c, and σ_3=108.14 MeV/c (remember FWHM=2.355σ).

The remaining portion of the article shows the process of correcting the Gaussians for a limited acceptance, and compares the predicted p_t distribution obtained from the three-Gaussian approximation (of the influence of the acceptance) with the analytical solution outlined in [3]. Our primary interest lies in the result for fragmentation experiments where there is an acceptance centered at 0-degrees. The fitting routine used to produce the 3-Gaussian fit is Minuit, part of the CERN library programs, and the uncertainty in each point is chosen as 0.1% of the peak value.

The next step is to consider the influence of the limited acceptance. Here we simply integrate the Gaussian distributions over the transverse acceptance limits of the Image 2 target box of the A1200 to find the transmission. These transmission coefficients are specifically calculated for fragments having a mean momentum of 3415 MeV/c and cannot be directly applied to other systems having different acceptance limits. If $P_x$limit=Sin(40 mrad/2)*3415 MeV/c and $P_y$limit=Sin(20 mrad/2)*3415 MeV/c, then the figure is generated from the equation,

$$\varepsilon = \int_{-\text{pylimit}}^{\text{pylimit}} \int_{-\text{pxlimit}}^{\text{pxlimit}} \frac{1}{2\pi\sigma^2} \exp\left(-\frac{\left(p_x^2 + p_y^2\right)}{2\sigma^2} \right) dp_x \, dp_y .$$

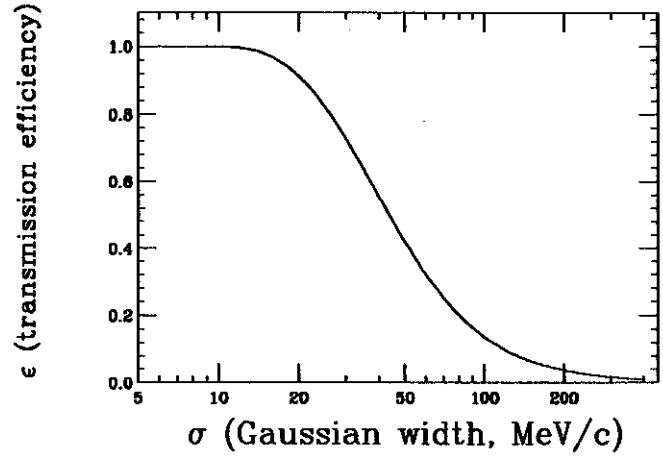

Figure 2. The efficiency of transmission through an acceptance equal to that of the Image 2 target chamber of the A1200 for a range of Gaussian distribution widths.

We now consider the transmission of the Gaussian distributions from the fit to the Lorentzian distribution. The transmission, ε, will be 96%, 61%, and 11% for the σ_1=14.63 MeV/c, σ_2=34.10 MeV/c, and σ_3=108.14 MeV/c components, respectively. Figure 3A shows the acceptance corrected, analytical solution for the Lorentzian distribution, seen as the long dashed line in Fig. 1 of [3]. The agreement is very good down to at least 1% of the peak height, showing that the approximate method is sufficiently accurate for all practical cases. The width of the corrected Lorentzian p_t distribution is 43.1 MeV/c FWHM, while the model predicts 43.3 MeV/c. The largest discrepancy is in the peak height of the distribution. In Figs. 3 and 4 both the analytic solution for the Lorentzian and the three-Gaussian estimate for the post acceptance distribution are shown on absolute scales with no normalization factors to show the accuracy with which the model can approximate a distribution.

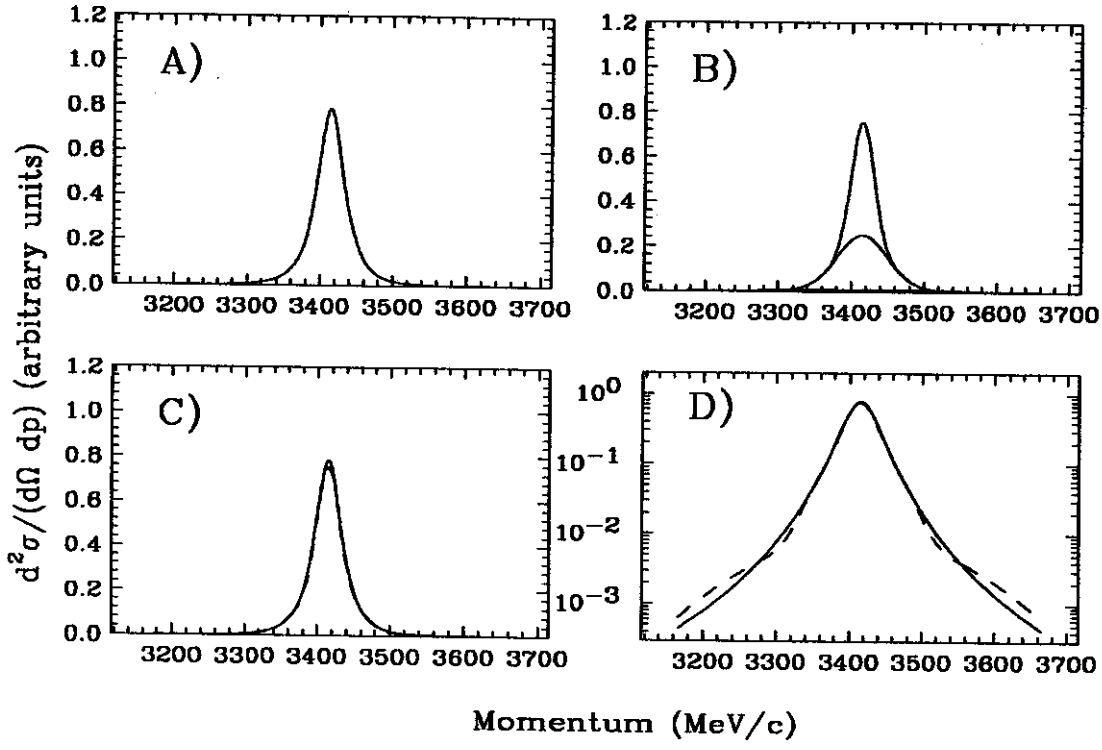

Figure 3. A comparison of the post acceptance analytical solution for a Lorentzian distribution, Γ=50 MeV/c, (A) and the post acceptance approximation from the three-Gaussian model (B). Figs 3C and 3D show a direct comparison of the two results.

The widths of the p_t momentum distributions of halo neutrons in ^{11}Li and ^{11}Be are of order 50 MeV/c, so the above analysis is representative of the interesting range. However, the results for a Lorentzian distribution with Γ=100 MeV/c also have acceptable accuracy; the three-Gaussian model and analytical solution yield widths of 76.3 MeV/c and 78.6 MeV/c, respectively.

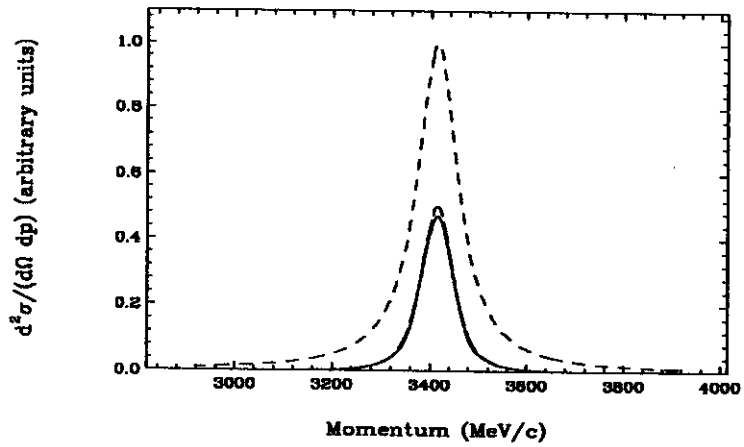

Figure 4. A Lorentzian p_t distribution with Γ=100 MeV/c (short dashed), compared with the analytical solution after passing through the Image 2 acceptance (long dashed) and the three-Gaussian post acceptance estimate (solid).

It is most interesting to apply the model to a more realistic momentum distribution, rather than the simple Lorentzian distribution. We consider the p_t distribution of the valence neutron of

^{11}Be predicted for a $1s_{1/2}$ neutron in a Woods-Saxon potential whose depth is adjusted to reproduce the 504 keV binding energy of ^{11}Be [4]. A three-Gaussian fit to the distribution, whose width is 45.4 MeV/c FWHM, yields Gaussians whose widths are σ_1=12.59 MeV/c, σ_2=22.28 MeV/c, and σ_3=58.66 MeV/c (A=5.04E-3, B=9.69E-3, C=1.33E-3). The correction for transmission through the limited acceptance narrows the width by 6% to 42.47 MeV/c. We have not yet found a way to test this approximation, though the ability of the method to accurately predict the acceptance effects for the Lorentzian distribution increases the confidence level for accepting this result.

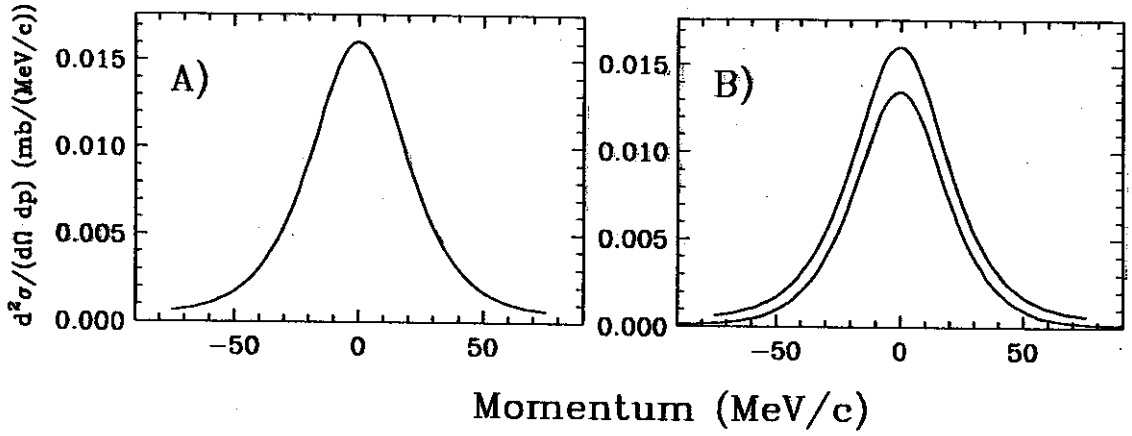

Figure 5. The p_t distribution of a $1s_{1/2}$ neutron bound by 504 keV in a Woods-Saxon potential is shown in 5A, with the three Gaussian best fit. Fig 5B shows the $1s_{1/2}$ neutron p_t distribution and compares with the three Gaussian approximation to show the (small) change in shape, and the losses from incomplete transmission of the distribution through the Image 2 acceptance.

A drawback to this method is the assumption that the momentum density distribution is symmetric in three dimensional space. Coulomb deflection, absorption, and other perturbations of the transverse momentum will distort the momentum density distribution, however these effects for light targets appear to be small [5]. Other problems arise when very small acceptances are used. This approach can produce meaningful results only when the momentum density distribution has a density that decreases as |p| increases. That is to say the momentum density distribution can have no relative minima, and must have a maximum value for p=0. In this case the p_t momentum distribution contains sufficient information to construct the 3-dimensional momentum density distribution.

In summary, we have developed a simple model to approximate the influence a limited transverse acceptance can have on the p_t distribution for fragments emitted with a Lorentzian momentum density distribution. The model predictions are in good agreement with the analytical solutions obtained by integrating the 3-dimensional Lorentzian density distribution over the transverse acceptance limits. The agreement between the analytical solution and the approximate method encourage the application of the three-Gaussian approximate method to estimate the influence of the limited acceptance on other momentum density distributions

References

1. N.A. Orr *et al.*, Phys. Rev. Lett. **69** (1992) 2050
2. K. Riisager, private communication.
3. J.H. Kelley *et al.*, elsewhere in this report.
4. H. Esbensen, private communication.
5. H. Sagawa and N. Takigawa, to be published in Phys. Rev. C.

PROTON DECAY FOLLOWING THE HEAVY ION TRANSFER REACTIONS ^{40}Ca (^{7}Li,^{6}He) ^{41}Sc*, ^{58}Ni(^{7}Li,^{6}He) ^{59} Cu*, and ^{90}Zr (^{7}Li,^{6}He) ^{91}Nb*

J. C. Staško, G.M. Crawley, S. A. Danczyk, J.E. Finck[a], S. Gales[b], H. Laurent[b], J. S. Winfield, and G.H. Yoo

A continuum, usually considered a "background", appears under any features observed at high excitation energy in single nucleon stripping reactions. An important part of the continuum arises from projectile breakup and evaporation of transferred particles.

Various attempts have been made to calculate the strength in the breakup continuum, including the use of the Serber model [1,2] and the use of a semiclassical approach developed by Bonaccorso and Brink [3,4]. The Serber model treats only the direct breakup process and uses simple geometrical arguments to obtain the breakup cross section. This model explains the continuum quite well in some light ion induced reactions but does not appear to work well for heavy ion stripping reactions [5,6,7]. The Bonaccorso-Brink approach treats the whole process of breakup and transfer simultaneously and has had some success in explaining at least the shape of the continuum for a number of heavy ion transfer reaction processes [7,8]. However, this approach predicts that for many heavy-ion induced reactions at energies above 20 MeV/A, most of the strength in the continuum arises from transfer into resonant states in the target and the subsequent decay of these states.

In the present experiment we explore the question of the continuum in the particular case of the reactions ^{40}Ca(^{7}Li,^{6}He)^{41}Sc*, ^{58}Ni(^{7}Li,^{6}He)^{59}Cu*, and ^{90}Zr(^{7}Li,^{6}He)^{91}Nb* at 50 MeV/A by measuring the angular distribution of the decay products of the resulting heavy nucleus above the proton threshold. The A1200 was used as a 0° spectrometer with the target at the normal second dispersive image position. The ^{6}He particles were detected near zero degrees in coincidence with the charged particles emitted at backward angles. The focal plane detectors consisted of a position sensitive Si detector (1 mm thick, 1 cm tall and 7 cm long) followed by a plastic scintillator. The particles detected in the focal plane were identified using the energy loss vs. total energy and time of flight vs. position two-dimensional spectra. The signal from the plastic scintillator was used as a start signal. The energy resolution for the ^{6}He spectra was about 500 keV full width at half maximum (FWHM.)

Eight 5 cm^2 Si detectors were placed around the target at a distance of 14 cm. Seven were placed at backward angles in the range of $110° \leq \theta \leq 160°$, and the eighth at $\theta = 32°$. ^{6}He nuclei were detected in coincidence with charged particles in the Si detectors. There were also seven BaF_2 detectors placed outside the target box in a stacked honeycomb pattern perpendicular to the target. The BaF_2 crystals were 24 cm long and had a hexagonal cross-section with a 3 cm face. The BaF_2 crystals detected γ rays, which were in coincidence with ^{6}He. The analysis of the γ-coincidence data is still in progress.

The singles spectra from the ^{40}Ca(^{7}Li,^{6}He), ^{58}Ni(^{7}Li,^{6}He), ^{90}Zr(^{7}Li,^{6}He) reactions obtained at zero degrees are displayed in Fig. 1 as well as the corresponding ^{6}He,p coincidence spectra, corrected for randoms. In each spectrum, the excitation energies corresponding to the proton and neutron thresholds, B_p and B_n, respectively, are marked with arrows.

The ^{40}Ca(^{7}Li,^{6}He) singles spectrum exhibits, besides the ground state, four peaks around 5.5 MeV, 8 MeV, 10.5 MeV and 12.5 MeV. These excitations have also been observed in other studies of ^{41}Sc [10]. Proton decay begins to occur at 1.1 MeV, but the coincidence spectrum will not show protons until around 4 MeV, because the threshold of the proton detectors was set to approximately 3 MeV. It is interesting to

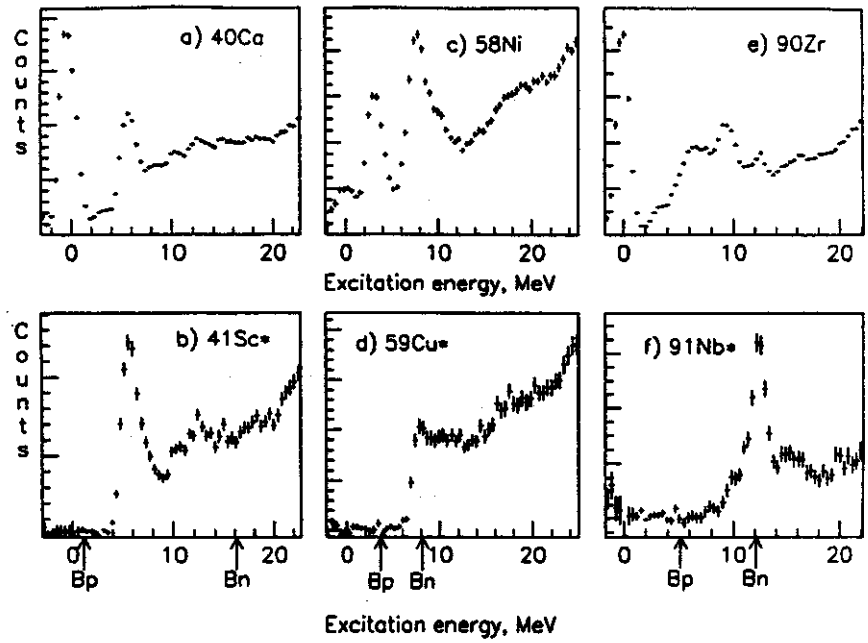

Figure 1: a) The ^{6}He singles spectrum for the ^{40}Ca(^{7}Li,^{6}He) reaction obtained at zero degrees and b) the ^{6}He coincidence spectrum obtained from the ^{40}Ca(^{7}Li,^{6}He)^{41}Sc* reaction at zero degrees. c) and d) are the singles and coincidence spectra for the ^{58}Ni(^{7}Li,^{6}He) and ^{58}Ni(^{7}Li,^{6}He)^{59}Cu* reactions, respectively, while e) and f) are the singles and coincidence spectra for the ^{90}Zr(^{7}Li,^{6}He) and ^{90}Zr(^{7}Li,^{6}He)^{91}Nb* reactions, respectively. The arrows indicate the energies corresponding to the proton and neutron thresholds.

note that the peak around 8 MeV seems to disappear in the coincidence spectrum. Neutron decay is not a possibility until the nucleus has 16.2 MeV of excitation energy. The ^{58}Ni(^{7}Li,^{6}He) singles spectrum exhibits two broad peaks at 3.5 MeV and 8.0 MeV, and also another possible unresolved peak at approximately 10 MeV. The broad feature at 3.5 MeV is a group of isobaric analog states, and the broad feature at 8 MeV is believed to be the same. Proton emission begins around 3.4 MeV and the neutron emission channel opens up at around 8.1 MeV. In the singles spectrum for the ^{90}Zr(^{7}Li,^{6}He) data, broad peaks are observed at excitation energies of 6.1 and 9.2 MeV. A single sharp peak is observed near 12 MeV in the coincidence spectrum. Presumably one or more of the states near 12 MeV have high spin and are favored by angular momentum matching in the (^{7}Li,^{6}He) reaction.

The measured values of the angular correlation R_p/R have been obtained directly, and are shown in Fig. 2. The angular correlation may be used to identify the states in the target nuclei which become populated with the transferred proton. Each of the plots shown are for energy regions that have large contributions to proton decay. The ^{41}Sc data displayed is for the energy region from 4.5 – 5.5 MeV, chosen because it is in the region of the first peak in the proton decay spectrum. The ^{59}Cu data, at 6.5 – 7.5 MeV, was chosen because it lies in the region where the protons are energetic enough to be detected and the neutron decay channel has not yet opened up. The ^{91}Nb data, at 11.5 – 12.5 MeV was chosen because it lies on the IAS around 12 MeV. The points in these plots at 32°, which are points from the forward detector are important because they indicate whether there is considerable breakup of the projectile. Direct breakup would exhibit an asymmetry in the angular correlation. This does not appear in the data shown. The angular correlations will allow us to study the population of the excited states in the nuclei and their decay by comparing with various models.

a. Physics Department, Central Michigan University, Mt. Pleasant, Michigan 48859
b. Institut de Physique Nucléaire, F91406, Orsay, France

References

1. R. Serber, Phys. Rev. 72, 1008(1948).
2. R. J. de Meijer, and R. Kamermans, Rev. of Mod. Phys., Vol. 57 No. 1, 147(1985).
3. A. Bonaccorso, D. M. Brink and L. Lo Monaco, J. Phys. G 13, 1407(1987).
4. A. Bonaccorso and D. M. Brink, Phys. Rev. C 38, 1776(1988).
5. J. R. Wu, C. C. Chang and H. D. Holmgren, Phys. Rev. C 19, 370(1979).
6. C. P. Massolo, et al., Phys. Rev. C 34, 1256(1986).
7. G. Yoo, G. M. Crawley, and J. S. Winfield, National Superconducting Cyclotron Laboratory Annual Report, 13(1989).
8. I. Lhenry, Ph. D. Thesis, Orsay (1992), unpublished.
9. F. Puhlhofer, Nucl. Phys. A 280, 267(1976).
10. J. Guillot, et al., Phys. Let. B 258, 3(1991).

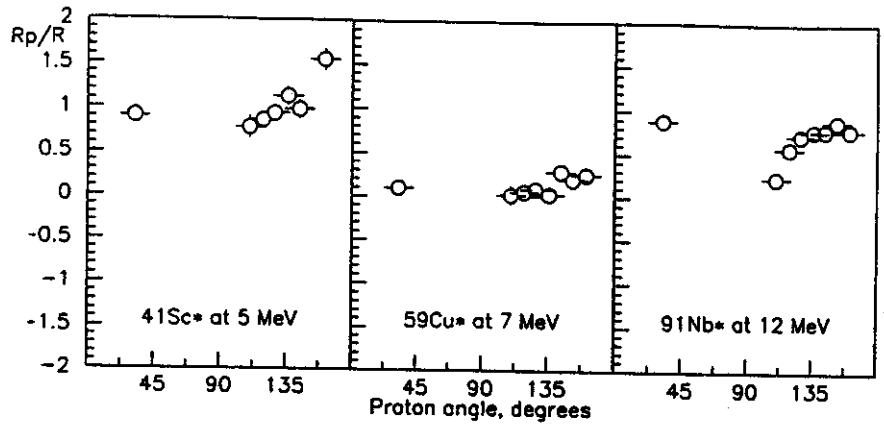

Figure 2: $W(\theta)$ for a) ^{41}Sc$\rightarrow p+^{40}$Ca at 4.5 – 5.5 MeV, b) ^{59}Cu$\rightarrow p+^{58}$Ni at 6.5 – 7.5 MeV, and c)^{91}Nb$\rightarrow p+^{90}$Zr at 11.5 – 12.5 MeV.

EXCITATION ENERGY DEPENDENCE OF THE GIANT DIPOLE RESONANCE WIDTH IN ^{120}Sn AND ^{208}Pb

T. Baumann, E. Ramakrishnan, A. Azhari, R. A. Kryger, R. Pfaff, M. Thoennessen, S. Yokoyama, J. R. Beene[a], F. E. Bertrand[a], M. L. Halbert[a], P. E. Mueller[a], D. W. Stracener[a], R. L. Varner[a], G. Van Buren[b], R. J. Charity[b], J. F. Dempsey[b], P-F. Hua[b], D. G. Sarantites[b] and L. G. Sobotka[b].

The study of Giant Dipole Resonances (GDR) built on highly excited states of nuclei provides valuable information about nuclear properties at high temperatures. So far the GDR in hot nuclei has been studied in many nuclei using fusion-evaporation reactions. The GDR is observed by measuring the decay of resonances built on highly excited states via high energy γ-ray emission. Fusion-evaporation measurements of the GDR in ^{110,112}Sn isotopes showed that the width of the resonance increases as a function of excitation energy [1], while the resonance energy stays nearly constant. Fusion reactions, however, form compound nuclei over a wide range of angular momentum states, and the average angular momentum increases with beam energy. The width increase observed in the GDR measurements in ^{110,112}Sn nuclei has therefore been attributed not to the rise of excitation energy but to deformation introduced in the compound nucleus at these high angular momenta [2]. It is not easy to decouple the effects of increasing angular momentum and excitation energy in fusion-evaporation reactions.

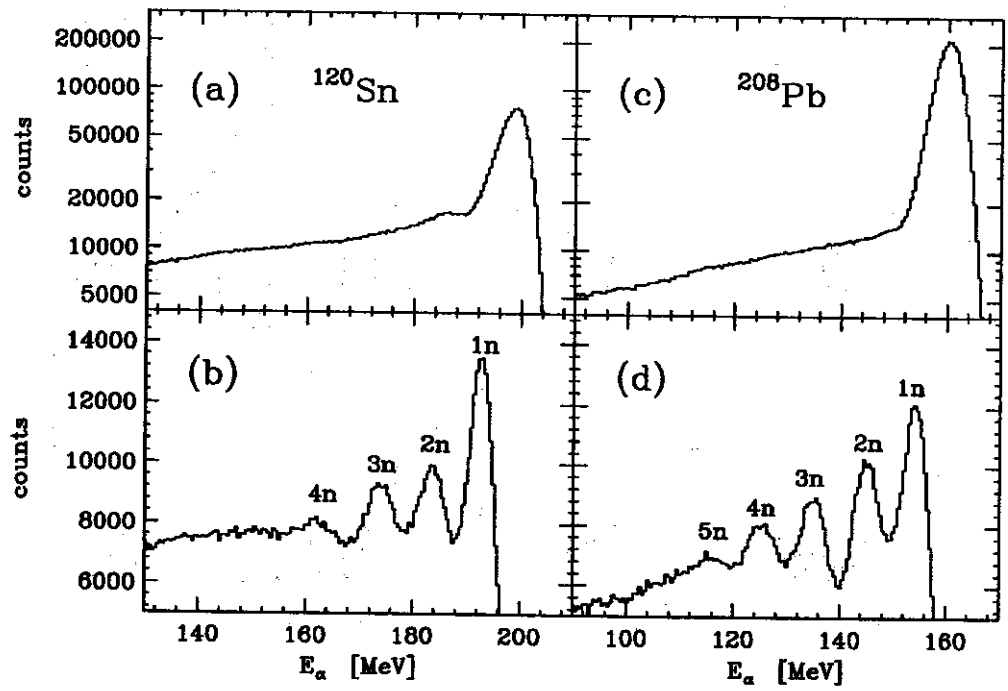

Figure 1: α-spectra of the Dwarf-Wall from the ^{208}Pb and the ^{120}Sn experiment; the top panels (a) & (c) show the α-singles spectra, the bottom panels (b) & (d) show α-spectra in coincidence with γ-rays. The structure in the coincidence spectra is due to the successive opening of neutron evaporation channels in the decay of the excited target nucleus.

We chose a different approach by exciting the nucleus of interest via light particle inelastic

scattering. At small forward angles, light ion inelastic scattering leaves the target in highly excited, low angular momentum states [3]. This enables us to study the GDR as a function of excitation energy, decoupled from angular momentum effects. Furthermore, by gating on different ranges of the inelastic spectrum of the projectile, we can study the GDR of the target nucleus over a wide range of excitations within one measurement.

The GDR of ^{208}Pb and ^{120}Sn was investigated in two experiments by measuring the high energy γ-rays from the decay of the resonance in coincidence with inelastically scattered α-projectiles. Both experiments were performed using the same experimental devices. α-beams with 160 MeV in the case of ^{208}Pb and 160 MeV and 200 MeV in the ^{120}Sn experiment were provided by the K1200 Cyclotron. The corresponding target was mounted at the center of the Washington University's *Dwarf-Ball/Wall* 4π detector array [4]. This array consists of CsI-scintillators and detected the scattered projectiles as well as other light charged particles. The 64 Ball detectors cover angles from 36° to 168° in the lab frame, the Wall array (35 detectors) has an enhanced resolution for forward angles from 10° to 36°. Particles in the Dwarf detectors were identified by pulse shape discrimination. Outside the scattering chamber five close-packed arrays with 19 BaF_2-detectors each (76 detectors from ORNL and 19 from NSCL) were placed at lab angles of 60°, 90° and 120°. These detectors measured the high energy γ-rays emitted by the GDR decay. γ-neutron separation was achieved by time of flight discrimination.

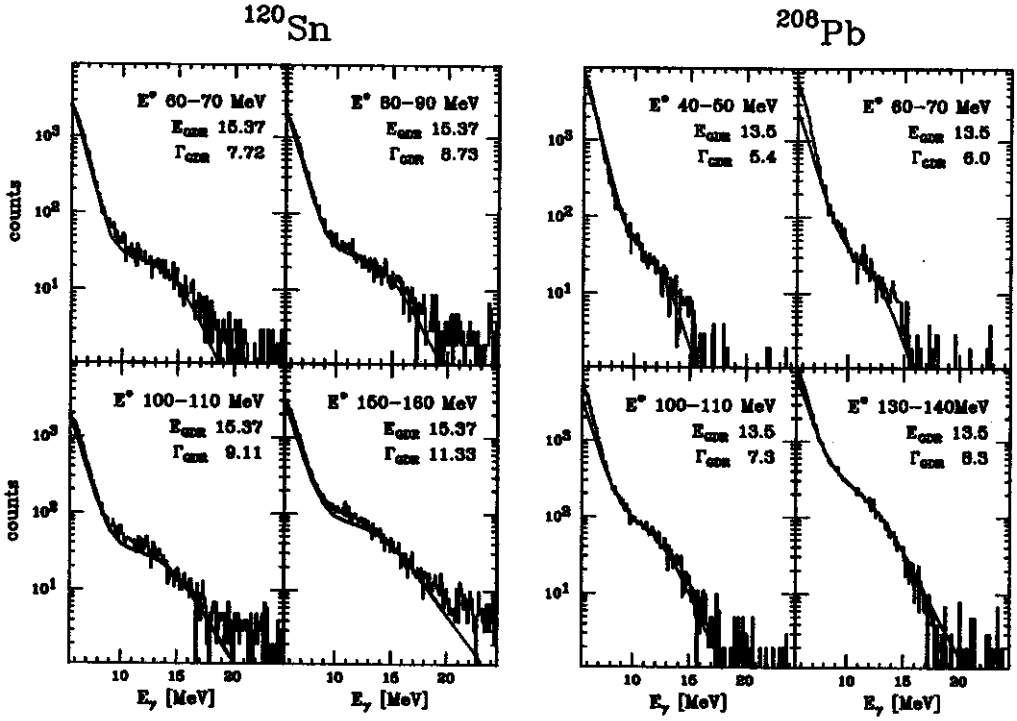

Figure 2: High energy γ-spectra for the ^{120}Sn (left) and the ^{208}Pb (right) experiment. The solid lines correspond to fits from CASCADE with the resonance energies and widths given in the panels.

In order to obtain the high energy γ-ray spectra from the GDR decay of the excited nucleus, the inelastic α-singles spectra (figure 1) were divided into energy bins of 10 MeV width corresponding to different excitation energies of the target nucleus.

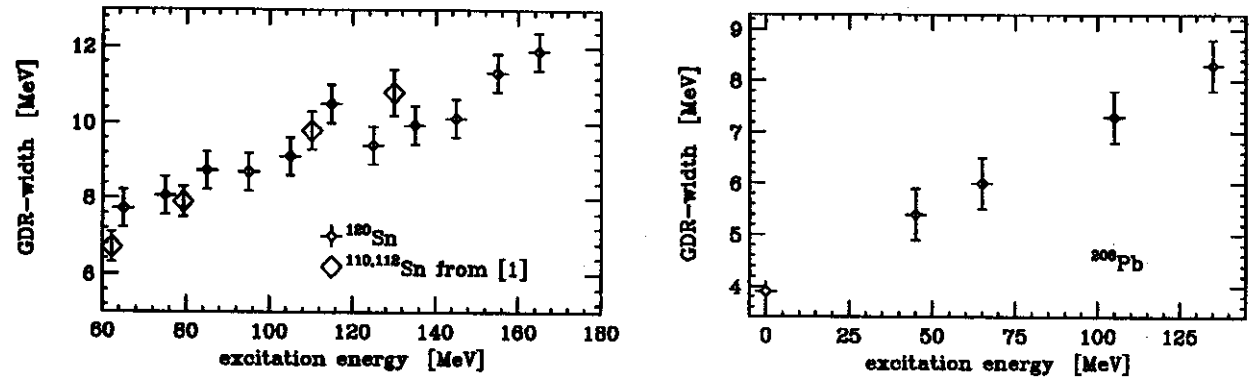

Figure 3: GDR widths versus target excitation energy; (left): in addition to our data on ^{120}Sn the fusion-evaporation data on ^{110,112}Sn-isotopes from [1] are included; (right): GDR-widths observed in the ^{208}Pb experiment.

This procedure also yielded the population distribution of excited nuclei within each energy interval, which we used as the input population for the statistical model code *CASCADE*. We then compare this simulation with our data. In a preliminary analysis we kept the GDR energy constant at the ground state value [5] and varied only the width. Four of these fits from each experiment are shown in figure 2.

Figure 3 shows that the GDR-width increases with excitation energy in both cases. The width increase observed in the ^{120}Sn case is similar to the results from the fusion-evaporation experiments on Sn-isotopes. Since inelastic scattering does not populate high angular momentum states, the observed width increase cannot be explained by target nucleus deformation due to an increasing angular momentum.

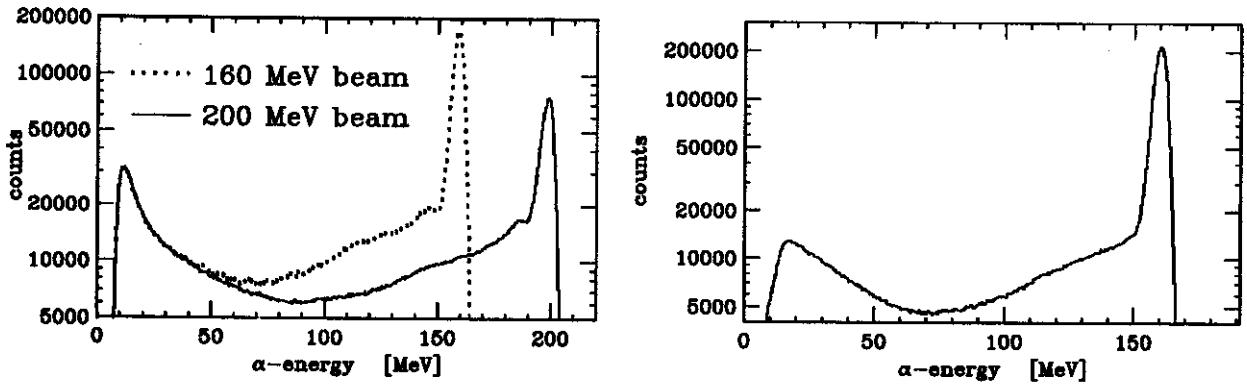

Figure 4: left: α-singles spectra from the ^{120}Sn experiment at 160 MeV and 200 MeV, the spectra are normalized in the lower energy region; right: α-singles spectrum from the ^{208}Pb experiment at 160 MeV.

Another surprising aspect of the data can be seen at low energies in the α-singles spectrum. The α-spectrum rises with decreasing α-energy. This was observed in both the ^{120}Sn and ^{208}Pb measurements. Furthermore, in the ^{120}Sn measurements this increase was compared for the two beam energies and was found to be identical (figure 4). This spectral shape at low α-energies cannot be explained with α-evaporation from an equilibrated target. Pre-equilibrium calculations using multi-step direct emission theory are currently underway.

a. Oak Ridge National Laboratory, Oak Ridge, Tennessee.
b. Dept. of Chemistry, Washington University.

References

1. D. R. Chakrabarty *et al.*, Phys. Rev. C 36, 1886 (1987).
2. A. Bracco *et al.*, Phys. Rev. Lett. 62, 2080 (1989).
3. M. Thoennessen *et al.*, Phys. Rev. C 43, R12 (1991).
4. D. W. Stracener *et al.*, Nucl. Instr. and Meth. A294 (1990).
5. S. Dietrich and B. Berman, At. Data Nucl. Data Tables 38, 208 (1988).

THE IDENTIFICATION OF NEW NUCLEI NEAR THE PROTON-DRIP LINE

M. Hencheck[a], R. N. Boyd[a,b], M. Hellström, D. J. Morrissey, M. J. Balbes[a], F. R. Chloupek[a], M. Fauerbach, C. A. Mitchell[a], R. Pfaff, C. F. Powell, G. Raimann[a], B. M. Sherrill, M. Steiner, J. Vandegriff[a], and S. J. Yennello[c]

The properties of proton-rich nuclei in the mass A = 90 range are of great interest to astrophysicists who model the rapid hydrogen burning process in very hot, dense stellar environments. However, little is known about many of the key nuclei that lie along the proton drip-line. The masses, lifetimes, and decay modes of these nuclei must therefore be estimated in order to include them in the calculation of the rp-process synthesis path. The uncertainties in the predicted ground state properties, together with a lack of knowledge about excited levels, which might serve as final states in beta-decay processes, are enough to produce large uncertainties in the resulting astrophysical calculations. In addition to this astrophysical interest, another motivation for the experimental interest in this mass region lies in the importance of mapping the exact location of the proton drip-line. The latter provides a crucial test of mass models and a means to determine how well a particular model can be used to extrapolate away from the valley of stability. The goal of the present work was to produce and identify new nuclei near the proton drip-line in the A = 80–100 region up to Z≈48, including the astrophysically very interesting silver isotopes ^{94,95}Ag. There exists a preliminary report of the observation of these isotopes at an on-line mass separator [1]. Based on these experiences it is reasonable to expect that future experiments, using heavier beams, will lead to the production of the doubly magic nucleus ^{100}Sn.

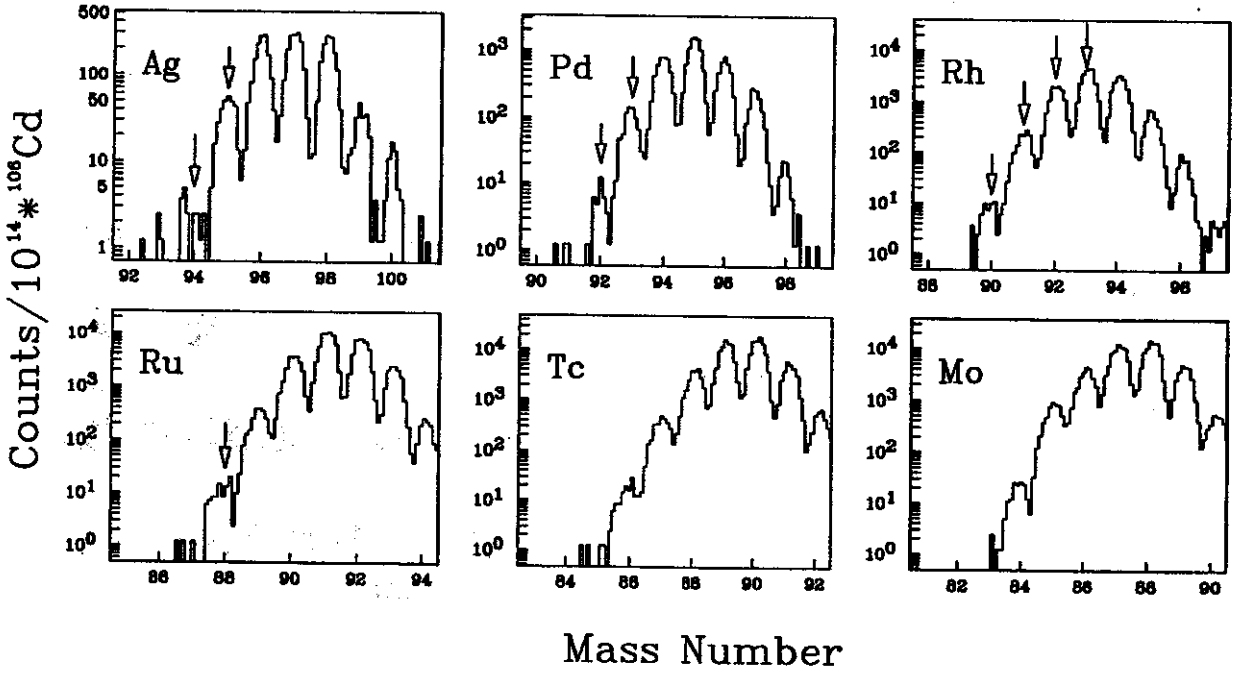

Figure 1: Mass spectra for Z=42–47 (molybdenum through silver). The number of counts have been normalized to 10^{14} beam particles incident on the production target. Nuclei identified for the first time in this study are indicated by arrows.

An E/A = 60 MeV beam of the rare isotope ^{106}Cd from the K1200 cyclotron was focused onto a 44.4 mg/cm^2 natural Ni target with a 9.4 mg/cm^2 ^{9}Be backing at the target position of the A1200 fragment

mass separator [2]. The ^{9}Be backing was used to increase the fraction of reaction products leaving the target in their fully stripped charge state. The reaction products were separated and identified using the A1200, employing standard experimental methods [3-5].

Information from two position-sensitive parallel-plate avalanche counters (PPACs) placed at the second dispersive image of the A1200 separator together with NMR measurements of the dipole fields of the separator were used to determine the magnetic rigidity of the product nuclei. Thin plastic scintillators at the first dispersive image and at the final focus were used to measure the time of flight (TOF) through the device and, hence, the velocity of the reaction products. A four element silicon telescope (ΔE_1, ΔE_2, E_1, E_2) placed at the focal plane of the A1200 provided two independent energy loss measurements as well as the total kinetic energy of the particles. The two energy-loss measurements allowed redundant determination of the atomic number Z of each ion by comparison of its position to that of the primary beam in the ΔE versus E_{total} coordinate space. A measurement of the charge state distribution of ^{106}Cd after the production target showed that $\approx$40% of the reaction products were fully stripped. The charge state Q of each ion was calculated by an appropriate combination of its magnetic rigidity, total kinetic energy, and velocity [3-5]. Consistency of the calculations was ensured by a comparison of the calculated Z with the calculated Q of the ions. Only fully stripped fragments, as selected by a narrow gate on Q=Z fragments, were used for the identification process. Histograms of ΔE versus TOF were prepared in which fragments with a given value of (N-Z) form "columns". For each column separately, the slope of the TOF as a function of 1/Z for the individual nuclides was calculated. For a given column, the ratio between its slope and the the average difference in slopes between adjacent columns is equal to the (N-Z) of that column, thus allowing an unambiguous determination of the mass number A of the fragments.

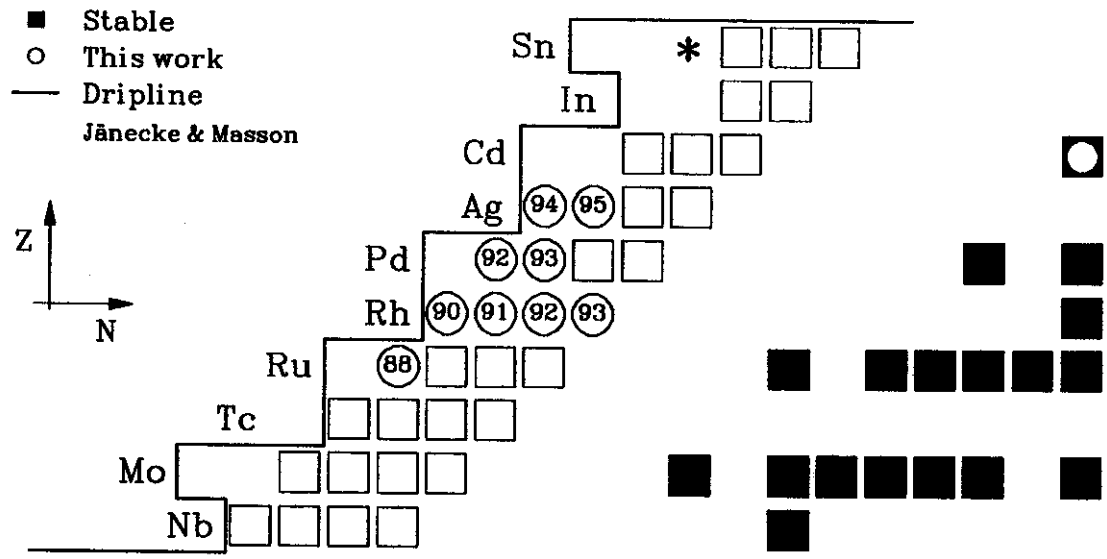

Figure 2: Section of the chart of the nuclides in the region of interest. Nuclei identified in the present work are circled. The doubly magic nucleus ^{100}Sn is indicated by an asterisk.

The mass spectra in Figure 1 show the identification and production rates of the new nuclei produced: ^{88}Ru, ^{90,91,92,93}Rh, ^{92,93}Pd, and ^{94,95}Ag. As can be seen in the figure, the mass resolution is sufficient to clearly separate the isotopes. A few events corresponding to ^{85}Tc, ^{87}Ru, ^{91}Pd, and ^{93}Ag are also

observed; however, it is difficult to conclude from such a small number of events whether these nuclei were in fact identified or whether these events were due to a background process. The data shown represent approximately 19 hours of data collection at a beam current of $\approx$ 0.2 pnA. The observation of an isotope in this experiment implies that the ion has a lifetime longer than its flight time through the A1200 separator, which is on the order of 150 ns.

Figure 2 shows a section of the chart of the nuclides in the region of interest (proton number Z = 40–50, mass A = 80–100). The drip-line prediction of Jänecke and Masson [6] is indicated by a solid line. Stable nuclei are indicated by black squares, and the projectile ^{106}Cd is specially noted. Open squares indicate previously known nuclei, while those nuclei identified for the first time in the present work are circled. Two of the new nuclei, ^{90}Rh and ^{94}Ag, are predicted to be the last proton stable isotopes of their respective elements. ^{94}Ag is the heaviest N=Z nucleus observed so far, three steps away along the N=Z line from the doubly magic nucleus ^{100}Sn.

The result for ^{95}Ag is of special astrophysical interest, since this isotope has recently been singled out as being particularly important in the nucleosynthesis of ^{92}Mo and ^{94}Mo [7]. These two molybdenum nuclei are unique among the "p-process" nuclides (nuclei which are blocked from production by the usual neutron capture processes) in that their isotopic abundances are relatively large, and their synthesis has remained a puzzle. In reference [7] it was shown that synthesis of the neutron deficient molybdenum isotopes could proceed via a series of rapid proton captures on preexisting material. However, the success of this model requires that ^{95}Ag be bound to insure that ^{92}Mo and ^{94}Mo be produced in the observed ratio. The present work thus supports this synthesis model.

a. Department of Physics, Ohio State University, Columbus, OH 43210
b. Department of Astronomy, Ohio State University, Columbus, OH 43210
c. Department of Chemistry, Texas A&M University, College Station, TX 77843

References

1. E. Roeckl, personal communication (1993).
2. B. Sherrill *et al.*, Nucl. Instr. Meth. Phys. Res. B56, 1106 (1991).
3. D. Bazin *et al.*, Nucl. Phys. A515, 349 (1990).
4. M. F. Mohar *et al.*, Phys. Rev. Lett. 66, 1571 (1991).
5. S. J. Yennello *et al.*, Phys. Rev. C 46, 2620 (1992).
6. J. Jänecke and P. Masson, At. Data Nucl. Data Tables 39, 265 (1988).
7. M. Hencheck *et al.*, submitted to Astrophys. J. (1994).

HALF-LIFE MEASUREMENTS OF RP-PROCESS NUCLEI

M. Hellström, J. A. Winger[a], W. Benenson, M. Fauerbach, R. A. Kryger, T. Kubo[b], D. J. Morrissey, R. Pfaff, C. F. Powell, B. M. Sherrill, M. Steiner, J. S. Winfield, and B. M. Young[c]

An important problem in nuclear physics today is to identify the limits of particle stability (the so-called driplines). In addition, measurements of the characteristics of the nuclei found there such as binding energies, half-lives to different types of decay, and structure of their (low-lying) excited states are important. The interest stems both from a need to test fundamental models of nuclear properties and from the implications that particle stability has on the extent of astrophysical nucleosynthesis processes. As the particle stability of proton-rich nuclei is severely limited by the Coulomb force, the proton drip-line lies much closer to the valley of beta stability than the neutron drip-line. The influence of the Coulomb barrier makes "exotic" decay modes possible, including beta-delayed one and multi-proton emission and, of course, direct one- and two-proton decay. It is also possible to study some aspects of nuclei *beyond* the driplines if their lifetimes are significantly longer than 10^{-22} seconds due to sufficently large Coulomb or angular momentum barriers [1].

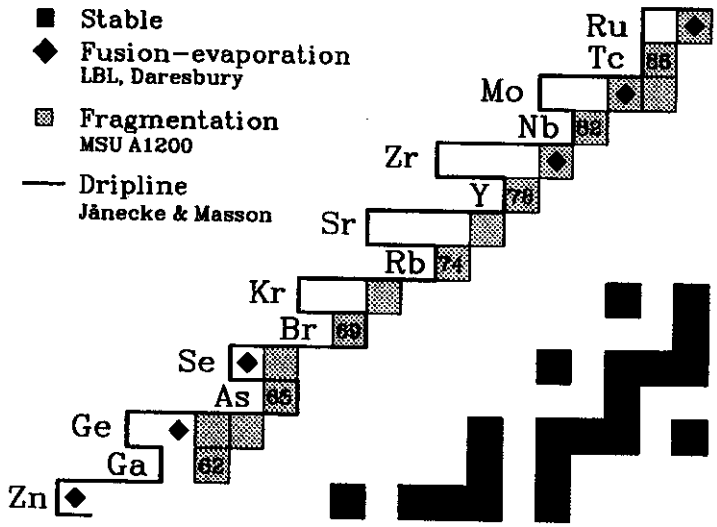

Figure 1: Section of the chart of the nuclides showing the proton-rich nuclei in the mass A=60-90 region

Projectile fragmentation at intermediate energies, as used at NSCL, GANIL, and GSI, has proved to be one suitable technique for producing nuclei far from stability [1], but fusion-evaporation reactions, e.g., (HI,pxn), at lower energies has also been used sucessfully [2], e.g., at LBL. However, in both methods the search for new isotopes is complicated by the presence of intense backgrounds of isotopes from other reaction channels and by low production rates. Figure 1 shows a section of the chart of the nuclides in the A=60-90 region, indicating the most neutron-deficient isotopes identified up to date. The solid line in the figure represents the prediction of the proton drip-line by the mass model of Jänecke and Masson [3].

The rapid proton-capture (rp) process can be viewed as an extension of the stellar nucleosynthesis models of the hot and cold CNO cycles, providing a path to proton-rich nuclei in the mass A=20-100 region

[4]. The high temperatures and densities required are thought to exist in several stellar and inter-stellar environments such as supernova shock waves and cataclysmic binary-star systems (novas and x-ray bursts). The latter case is characterized by the accretion of material from a companion star orbiting a massive object such as a neutron star or a black hole. The gravitational pull causes the temperature and density of the accreted material to reach a critical point, at which thermonuclear runaway occurs. The resulting particle flux leads to synthesis of new nuclei. The extent of the process depends on the starting material ("metal" content) and time scale of the burning. The process follows a path of alternating proton/alpha captures and beta decays. If the product of a capture reaction is proton-unstable, the process must wait for the precursor to beta-decay. If the beta decay half-life is long compared to the total timescale of the thermonuclear event (typically 2-500 s) the rp-process will terminate. Using data from various dripline predictions ^{65}As, ^{69}Br, and ^{73}Rb have been identified as potential termination points [4].

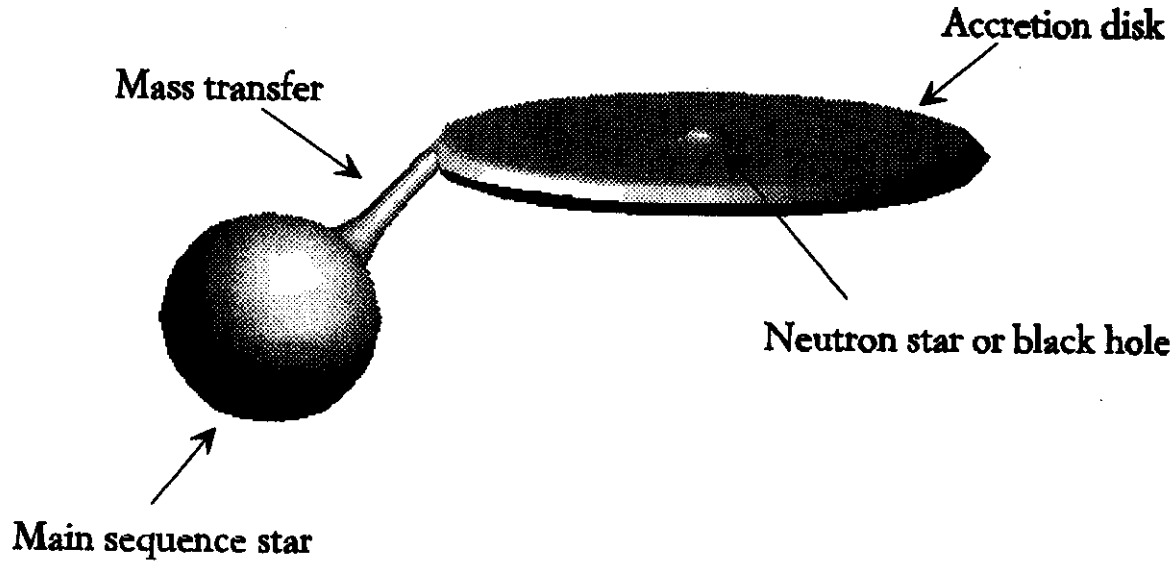

Figure 2: A binary system consisting of a very dense object, such as a neutron star or a black hole, accreting mass off a nearby main sequence star. The conditions inside the disk can lead to rapid proton capture and thus synthesis of mass A=20-100 nuclei.

In one of the first experiments with the A1200 separator at NSCL, Mohar *et al.* [5] identified both ^{65}As and ^{69}Br from fragmentation of ^{78}Kr at 65 MeV/nucleon. However, the observation of a nuclide is not an absolute proof for particle stability: as long as the lifetime of the nucleus towards particle emission is on the order of its flight-time through the experimental apparatus it will be observed. A more definitive proof of the location of the dripline can therefore really only be achieved by observation of direct proton radioactivity. Several authors [6,7] have searched for ground state proton decays for both ^{65}As and ^{69}Br but with negative results. The failure to observe protons could be attributed either to beta decay being the predominant decay mode for both these nuclei, or to low production cross sections (fusion-evaporation reactions were used) and/or the proton decay half-lives being too short to be detected with the experimental setups used. To clarify the situation for ^{65}As, Winger *et al.* [8] measured the beta decay half-lives for several nuclei in the mass A=60-70 region. The results for ^{65}As show that the primary decay mode is beta emission, with a half-life of 190(11) ms, meaning that proton capture to produce ^{66}Se should be possible. The observed half-life puts a lower limit of $S(p) \geq -250$ keV on the proton separation energy (in case the ground state is proton unbound).

In April of 1993, we made an attempt to measure the beta decay half-life of ^{69}Br using the technique of Winger *et al.*. Proton-rich reaction products produced in the fragmentation of ^{78}Kr at 70 MeV/nucleon on a natural Ni target were separated using the A1200 separator [9]. By placing an achromatic energy degrader at the second dispersive image, the number of fragment species reaching the focal plane of the device was reduced from several hundred to 10-15. The detector setup placed at the focal plane is shown schematically in Figure 3. The fragments were implanted in a four-element silicon detector telescope designed so that the nuclides of interest stopped in the third element. Since it is expected [8] that the beta decays of $T_z = 1/2$ nuclei like ^{69}Br primarily will proceed via allowed ground state to ground state transitions with high Q_β values, the telescope was mounted in a copper cylinder which thickness was selected to stop low- energy beta particles (cut-off $\approx$ 4 MeV) in order to suppress the background from low-Q_β events. A cylindrical thin plastic scintillator and a large block of plastic scintillator subdivided into four optically insulated quadrants surrounded the telescope. Each of the plastic detectors had its own photo-multiplier readout.

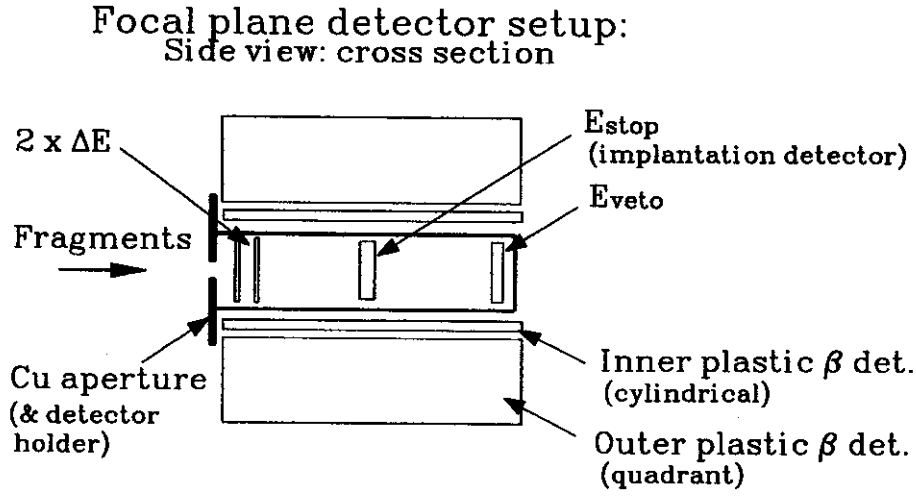

Figure 3: Schematic cross section view of the focal plane detector setup. See the text for details.

The data acquisition system was set up to check the energy loss and time of flight for each implanted fragment. If these parameters were within limits set in software, the cyclotron was dephased ("beam off") and the time recorded. During the next 500 ms, the energy signals and the time (relative to the start of the beam off period) of all coincidence events between the inner cylinder and *one* of the outer quadrant detectors were recorded. The coincidence requirement served to suppress cosmic ray events and room background. At the end of the 500 ms interval the beam was automatically turned back on and the process repeated.

The decay events associated with a certain nuclide were selected by applying cuts in the energy loss and TOF of the implanted nuclei. By looking at the resulting time distribution of the decay events associated with long-lived nuclei with low beta decay energies, the level of the background due to random coincidences could be assessed. This result, scaled by the number of valid implantations of the respective nuclei, could then be applied to the decay time spectra of short-lived, high Q_β nuclei. The left panel of Figure 4 shows the decay time spectrum obtained by gating on ^{68}Se ($T_{1/2}$ = 1.6 min, Q_β = 4.8 MeV). The right panel shows the corresponding distribution for ^{70}Br (Q_β = 10.4 MeV). The half-life for ^{70}Br obtained

by fitting the decay curve with the maximum likelihood fitting routine of Winger *et al.* [8] is 68(11) ms is in fair agreement with the value of Burch *et al.* [10] of 78.54(59) ms.

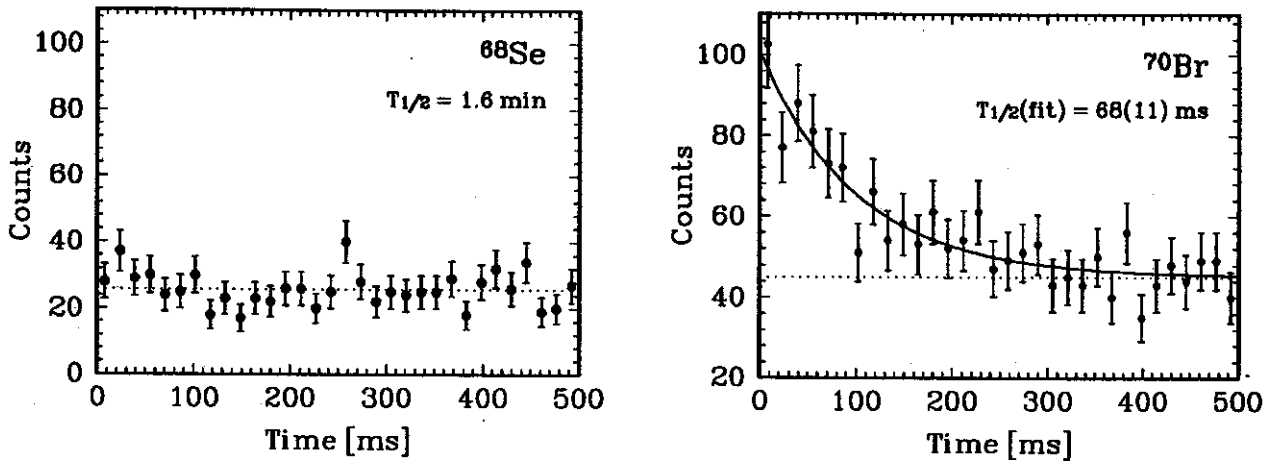

Figure 4: Decay time spectra for ^{68}Se (left) and ^{70}Br (right). See the text for details.

Unfortunately, no result for the beta decay half-life of ^{69}Br could be obtained in this experiment, in part due to its low countrate. Robertson *et al.* [7] argue that if the half-life of this nucleus is above 100 ms, positron decay would be the dominant decay mode. This places a lower limit of $\approx$ 300 keV on the energy of any emitted protons from the ground state decay. If, like ^{65}As, ^{69}Br proves to have a half-life on the order of 100 ms, it is likely that the rp-process will be able to proceed to ^{70}Kr and beyond. Experiments by D'Auria *et al.* [11] at ISOLDE and later by Yennello *et al.* [12] at NSCL show that ^{74}Rb most likely is the lightest proton-bound rubidium isotope This would make further proton captures on ^{72}Kr to produce ^{73}Rb impossible. Since the beta decay half-life of this nucleus is quite long (17 s), it is likely that ^{73}Rb represents the ultimate termination point of the rapid proton-capture process.

a. Present address: Mississippi State University, Department of Physics, Mississippi State, Mississippi
b. Present address: Cyclotron Laboratory, RIKEN, Wako, Saitama, Japan
c. Present address: A. W. Wright Nuclear Structure Laboratory, Yale University, New Haven, Connecticut

References

1. A. Mueller and B. M. Sherrill, Annu. Rev. Nucl. Part. Sci. 43 (1993) 529 and references therein.
2. J. C. Batchelder *et al.*, Phys. Rev. C48 (1993) 2593 and references therein.
3. J. Jänecke and P. J. Masson, At. Data Nucl. Data Tables 39 (1988) 265.
4. A. E. Champagne and M. Wiescher, Annu. Rev. Nucl. Part. Sci. 42 (1992) 39 and references therein.
5. M. F. Mohar *et al.*, Phys. Rev. Lett. 66 (1991) 1571.
6. E. Hourani *et al.*, Z. Phys. A334 (1989) 277.
7. J. D. Robertson *et al.*, Phys. Rev. C42 (1990) 1922.
8. J. A Winger *et al.* Phys. Lett. 299B (1993) 214 and Phys. Rev. C 48 (1993) 3097.
9. B. M. Sherrill *et al.*, Nucl. Instrum. Meth. B56/57 (1991) 1106.
10. R. H. Burch *et al.*, Phys. Rev. C 38 (1988) 1365.
11. J. D'Auria *et al.*, Phys. Lett. 66B (1977) 233.
12. S. J. Yennello *et al.*, Phys. Rev. C 46 (1992) 2620.

^{132,133}Pr ROTATIONAL BAND EXTENSIONS FROM THE ^{37}Cl ON ^{100}Mo REACTION

C.V. Hampton, Aracelys Rios, W.A. Olivier, R.M. Ronningen, Wm.C. McHarris and ORNL Nuclear Structure Research group.

In past years, results have been presented for the 160-MeV reaction ^{100}Mo(^{37}Cl,5nγ)^{132}Pr, performed with the Compton Suppression γ-ray Spectrometer at Oak Ridge National Lab.

We have now extended the rotational band scheme of what[1] has been referred to as a doubly decoupled band in ^{132}Pr, based on a $\pi h_{11/2} \otimes \nu i_{13/2}$ orbital coupling. Figure 1 shows the spectrum from a 2-D Multiple gate. Events in coincidence with the γ-ray spectra from four major transitions (116, 130, 178, 283 keV) were scanned into a 2-D array; then selected energy gates were summed to represent the band. Figure 1 represents a sum of transitions in ^{132}Pr that have been noise filtered using a FFT technique, background subtracted and baselined. The width and the bimodal appearance of the peak centered at 1009 keV suggest that there are actually two transitions present, separated by about 2 keV. This indicates that backbending is occurring at this point. The sequence may be 913, 1011, 1008, 1114 keV. However, because of the presence of many low intensity peaks, there is the possibility that the backbend extends lower in energy, beyond the 1008 keV transition.

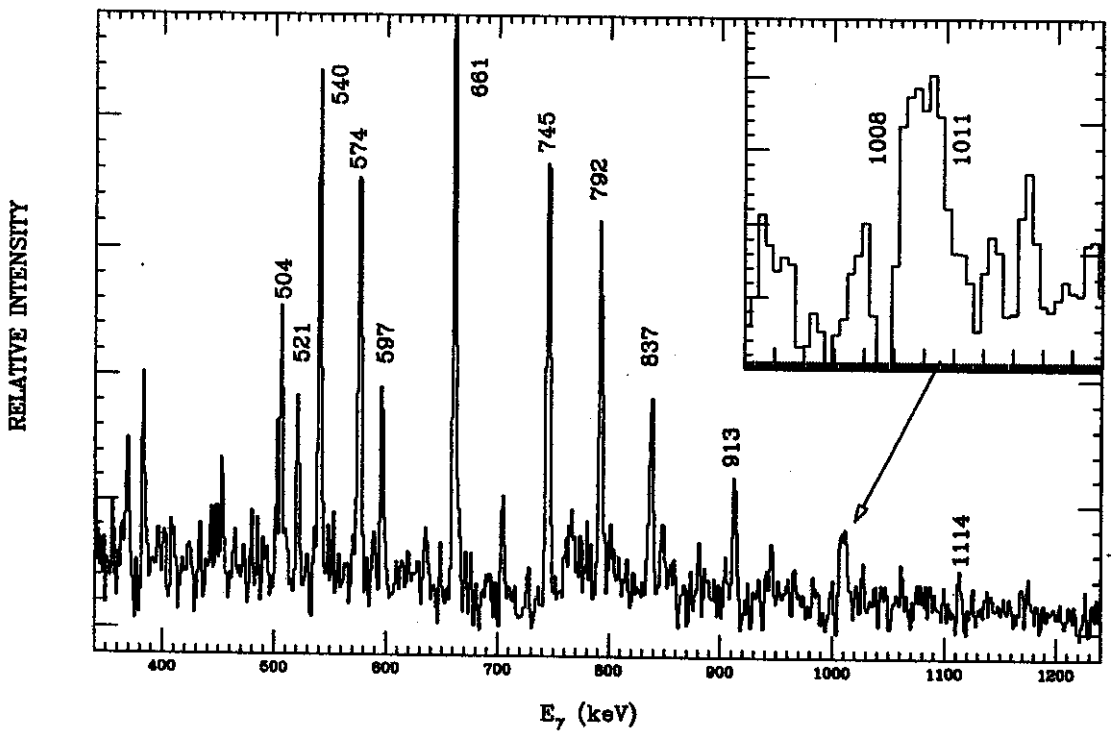

Figure 1: ^{132}Pr spectrum representing rotational band 3, from a 2-D multiple gate technique. The upper right hand corner contains an expanded view of the 1008 and 1011 keV peaks.

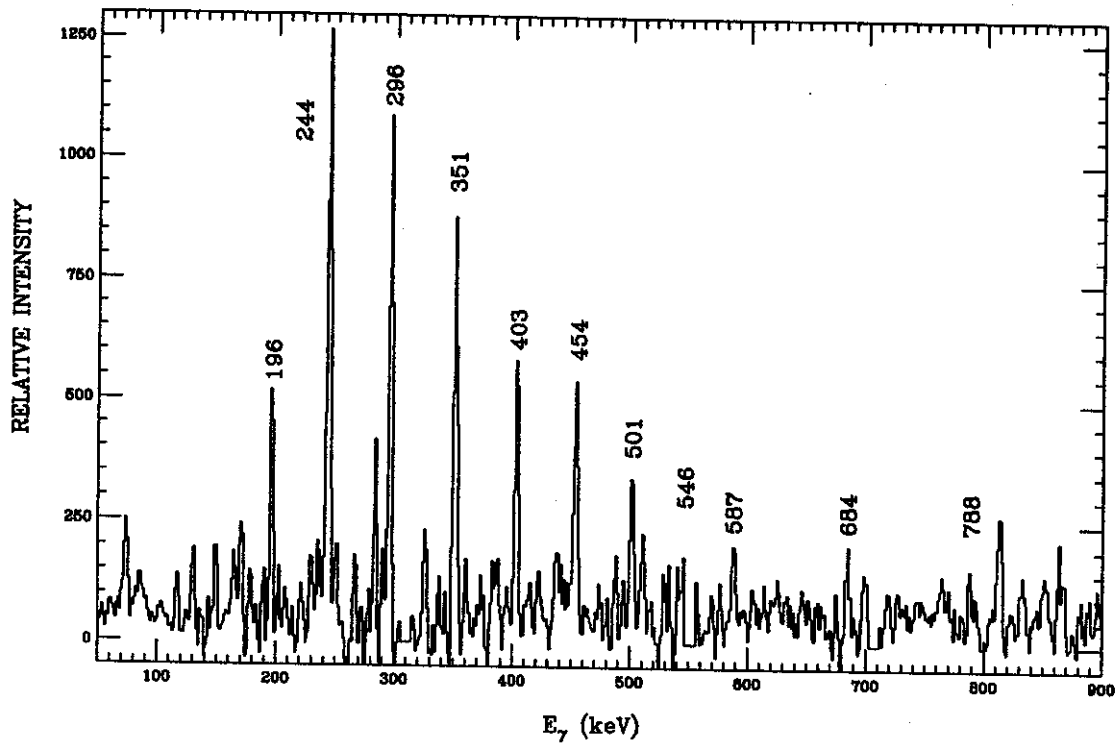

Figure 2: ^{133}Pr spectrum representing rotational band 6, from a 2-D multiple gate technique. (The 546 keV peak has been partially erased by the 551 keV primary gate.)

During the same experiment, rotational bands were also obtained from the ^{100}Mo(^{37}Cl,4nγ)^{133}Pr reaction. The ^{133}Pr nucleus had previously been studied under lower spin conditions.[2-4] We present information using a simple and a multiple gate technique to extend the band, designated collective oblate[3], by a few energy transitions. This band has been designated the $\pi h_{11/2} \otimes (\nu h_{11/2})^n$ orbital configuration.

Triples events in coincidence with spectra from three major transitions (310, 551, 709 keV) were scanned into a 2-D array. Then selected energy gates from this array were summed to represent the band. Figure 2 is a spectrum representing rotational band 6 for ^{133}Pr. It was produced by the 2-D multiple gate technique. This band has been published before.[4] The reported sequence is 196, 244, 296, 351, 403, 454, 501, 546, 587, 626, 662, 686 keV. The low intensity segment, after 587 keV, is in dispute with our results. While we do see peaks at 626 and 662 keV using our simple gate technique, these peaks disappear when using our, more selective, 2-D multiple gate technique. The sequence is more likely concluded with: 587, 684, 788 keV.

References

1. S. Shi, et al.,Phys. Rev. C *37*, (1988) 1478.
2. L. Hildingsson et. al, Phys. Rev. C., *33*, (1986) 2200.
3. L. Hildingsson et. al, Phys. Rev. C., *37*, (1988) 985.
4. D.B. Fossan et.al, Nuc. Phys. A, *520*, (1990) 241c.